RESEARCH ARTICLE

Key Points:
- Melt pond formation on first year sea ice is enhanced by freshwater refreezing as it flows through ice porosity, blocking percolation
- Ice temperature and freshwater availability during melt onset control percolation blockage, influencing the extent of melt pond formation
- The relationship between pond formation and ice temperature may be exploited to improve models of summer sea ice albedo

Correspondence to:
C. Polashenski,
chris.polashenski@gmail.com

Percolation blockage: A process that enables melt pond formation on first year Arctic sea ice

Chris Polashenski[1,2] (ID), Kenneth M. Golden[3] (ID), Donald K. Perovich[2,4] (ID), Eric Skyllingstad[5] (ID), Alexandra Arnsten[2], Carolyn Stwertka[2] (ID), and Nicholas Wright[2] (ID)

[1]USACE-CRREL Alaska Projects Office, Ft Wainwright Alaska, USA, [2]Dartmouth College, Thayer School of Engineering, Hanover, New Hampshire, USA, [3]Department of Mathematics, University of Utah, Salt Lake City, Utah, USA, [4]USACE-CRREL, Hanover, New Hampshire, USA, [5]Oregon State University, College of Earth, Ocean, and Atmospheric Sciences, Corvallis, Oregon, USA

Abstract Melt pond formation atop Arctic sea ice is a primary control of shortwave energy balance in the Arctic Ocean. During late spring and summer, the ponds determine sea ice albedo and how much solar radiation is transmitted into the upper ocean through the sea ice. The initial formation of ponds requires that melt water be retained above sea level on the ice surface. Both theory and observations, however, show that first year sea ice is so highly porous prior to the formation of melt ponds that multiday retention of water above hydraulic equilibrium should not be possible. Here we present results of percolation experiments that identify and directly demonstrate a mechanism allowing melt pond formation. The infiltration of fresh water into the pore structure of sea ice is responsible for blocking percolation pathways with ice, sealing the ice against water percolation, and allowing water to pool above sea level. We demonstrate that this mechanism is dependent on fresh water availability, known to be predominantly from snowmelt, and ice temperature at melt onset. We argue that the blockage process has the potential to exert significant control over interannual variability in ice albedo. Finally, we suggest that incorporating the mechanism into models would enhance their physical realism. Full treatment would be complex. We provide a simple temperature threshold-based scheme that may be used to incorporate percolation blockage behavior into existing model frameworks.

1. Introduction

Surface melt begins on Arctic sea ice in the late spring, producing meltwater that is retained on the ice in pools called melt ponds. These melt ponds are one of the most iconic and important features of the summer Arctic sea ice, dramatically reducing the ice albedo and enhancing transmission of light into the upper ocean by reducing the backscattering of light from exposed ice [*Perovich et al.*, 2002; *Perovich and Polashenski*, 2012]. In this way, ponds control both the energy balance of the ice-ocean system [*Curry et al.*, 1995] and the availability of light for primary productivity beneath the ice [*Nicolaus et al.*, 2012; *Frey et al.*, 2011; *Arrigo et al.*, 2012]. While optical properties of individual ponds vary, the areal fraction of the surface that the ponds cover is by far the most important aspect of pond formation in determining spatially averaged albedo and solar partitioning [*Polashenski et al.*, 2012].

A primary control over the evolution of pond coverage is the existence of pathways for water exchange through the ice. On first year sea ice, early in the melt season, pond coverage is largely controlled by a hydraulic balance of meltwater inflows and outflows and the bathymetry of the depressions available for this water to pool in [*Eicken et al.*, 2002; *Polashenski et al.*, 2012]. Limited outflow pathways result in an accumulation of meltwater above sea level and large pond coverage on undeformed ice. Later in the melt season, pathways for water to pass between the ice surface and ocean become relatively unrestricted, first through the formation of large drainage holes, and later through the onset of permeability through the ice matrix [*Polashenski et al.*, 2012]. After large levels of permeability are established, pond coverage is controlled by the fraction of the ice surface situated below sea level [*Polashenski et al.*, 2012]. The timing of the transitions in pond evolution on first year ice is therefore heavily dependent on the particulars of ice permeability.

Melt pond formation above sea level on first year ice could be considered counterintuitive upon first inspection. First year sea ice is highly porous near its melting point [*Weeks and Ackley*, 1986]; too porous, it would seem, to retain meltwater above hydrostatic equilibrium. A wide range of measurements of the permeability of sea ice, as well as theoretical modeling of percolation processes, indicates that sea ice permeability can be predicted from its brine volume fraction or gross porosity [*Golden et al.*, 1998, 2007; *Eicken et al.*, 2002; *Petrich et al.*, 2006; *Freitag and Eicken*, 2003]. Porosity is, in turn, directly related to the temperature and salinity of the ice [*Frankenstein and Garner*, 1967]. As the temperature of sea ice rises, the volume of brine pockets retained in the ice grows to maintain the brine pocket contents at their salinity-determined freezing point. This results in large increases in the porosity of sea ice as temperature increases [*Frankenstein and Garner*, 1967]. Whenever porosity exceeds a critical threshold (i.e., 5% for columnar first year ice [*Golden et al.*, 1998], or about 10% for granular first year ice [*Golden*, 2003]) both permeability theory and observations indicate that the liquid inclusions become connective and percolation pathways through the ice become available for the drainage of meltwater.

The dilemma posed by the above-sea-level formation of ponds on first year ice is that temperature and salinity observations indicate porosity is typically well above percolation thresholds prior to and during the formation of melt ponds [*Polashenski et al.*, 2012; *Landy et al.*, 2014]. The ice should, therefore, be abundantly permeable when meltwater begins to form, and any meltwater above hydrostatic equilibrium should rapidly drain. Boreholes drilled partly through the sea ice prior to and during the onset of ponding quickly flood with seawater rushing in from below, confirming this expected high permeability [*Polashenski et al.*, 2012].

Several possible explanations have been set forth to explain the process of pond formation above sea level on otherwise highly permeable ice. These include, (1) reduced pore connectivity in the granular ice layer (with correspondingly greater percolation threshold), (2) formation of impermeable superimposed ice layers as melt refreezes on top of the original sea ice surface, and (3) formation of interposed ice plugs within connective brine pathways when intruding meltwater freezes within the matrix of the sea ice [*Golden et al.*, 2007; *Eicken et al.*, 2004; *Freitag and Eicken*, 2003; *Polashenski et al.*, 2012]. Each of these likely has an impact on ice permeability, and the relative magnitude of these impacts likely varies from season to season and between ice types. The first two mechanisms, however, are inadequate to explain pond formation above sea level on first year sea ice in at least some cases. Porosity, as determined by temperature and salinity measurements, has been observed to exceed even a larger (10%) granular ice permeability threshold [*Golden*, 2003] prior to the onset of ponding, and partial removal of superimposed ice has been found to occur prior to the drainage of ponds [e.g., *Polashenski et al.*, 2012; *Landy et al.*, 2014]. Both superimposed ice formation (meltwater refreezing on top of the ice in a discrete layer) and interposed ice formation (meltwater refreezing within the ice pore space) are governed by similar underlying temperature-salinity dynamics. The key difference in terms of pond formation is that interposed ice could potentially block percolation through sea ice even after significant surface ablation has occurred, removing any discrete impermeable surface layer, and could repair new flaws which become connective through the ice due to ongoing internal melt. Here we present results that confirm the existence of this third mechanism and discuss its importance. We demonstrate the formation of ice "plugs" within the porous matrix of the sea ice as fresh water intrudes from above and replaces brine pockets. We then explore the conditions of intruding water and internal ice temperature that control percolation blockage. The results suggest that this internal pore blockage is an essential process, required to explain the extended time that ponds have been observed to remain above-sea level on first year sea ice [*Polashenski et al.*, 2012; *Landy et al.*, 2014]. We discuss how the formation of above-sea-level ponds controls the existence of ponds later in the melt season, demonstrating the durable impacts of this process on energy balance. Further analysis finds that the salinity of intruding meltwater, controlled by at least in part by snow availability, and the temperature of the sea ice interior at the time of surface melt onset are primary factors in controlling water retention in melt ponds on first year sea ice. We suggest the connection to ice interior temperature may be exploited to represent the abrupt transition observed from nearly impermeable to highly permeable in model parameterizations. We conclude by suggesting that this process of refreezing meltwater within the pore space of sea ice should be considered in future revisions of melt pond water retention schemes of GCM's, potentially enabling them to capture an important mechanism driving interannual variability of sea ice loss.

2. Methods

2.1. Sites and Conditions

We observed the permeability of undeformed first year sea ice at multiple locations throughout the southern Chukchi Sea from 18 May to 17 June 2014. This period bridged the transition from cold snow covered sea ice, through melt onset, and into the earliest stages of melt pond formation. At the start of this time period, the ice had already warmed above approximately $-2.7°C$ throughout the vertical profile, and desalination of the uppermost sea ice layers, particularly those above sea level, was observed at all sites. Minimum porosity of the ice, as derived from its minimum internal temperature ($>-2.7°C$) and salinity ($\sim$4–6 PSU), exceeded 10% at all locations. The large porosity was expected to indicate that the ice had a highly connected internal brine structure, and that the ice was very permeable, even at this time prior to meltwater production [Golden et al., 2007]. Site locations were within the area from 69.5 to 73.2°N latitude and 161.9 to 168.7°W longitude (see Table 1). Ice sampling within this area was largely driven by program goals unrelated to this work. Spatial progression of the experiment, particularly north and south, adds variability to the temporal change seen in many variables (i.e., ice temperature). This produces a record containing small apparent reversals or accelerations of spring evolution as ship movement across latitude-added spatial variability to the temporal sequence. Individual floes were selected to represent undeformed first year sea ice of the highest locally available thickness class. Mean and modal ice thickness and mean snow depth at each site are presented in Table 1. These were established along 100–200 m transect lines with an EM-31 [Eicken et al., 2001] and Magnaprobe [Sturm and Holmgren, 1999; Marshall et al., 2006], respectively. Accuracy of average observations of ice thickness are ±0.1 m and those of snow depth are ±0.01 m. Individual readings of both instruments are within ±0.03 of manual probe observations for the magnaprobe (95% level) and within $\pm$ 0.3 (95% level) for level ice with the EM-31. The largest sources of error are over/under probing for the magnaprobe and variability of ice thickness within the $\sim$5 m footprint of the EM-31. Typical floes had mean and modal ice thickness just under a meter, thinner than would be expected for full-winter thermodynamic growth in the region. This may be reflective of what appeared to be a stronger than average pattern of offshore ice movement, coastal lead opening, and ice generation during in the Chukchi Sea during the previous winter. Sea ice conditions in the region during the cruise, as recorded by observers on the bridge using the ASSIST protocol [http://icewatch.gina.alaska.edu/] (Figure 1) provide more context and confirm that the floes sampled were representative of the most common ice type in the region—first year ice of $\sim$1 m thickness. Limited climatology is available for snow depths in the region [Webster et al., 2014], but we are inclined to think that the average snow depths we observed (Table 1 and Figure 1a) were thin relative to average based on our field experience in the region, possibly due to later winter formation of much of the ice we worked on. Ice thickness at the exact location of the bores tended to be thicker than

Table 1. Ice and Snow Observations at Sites

Date (2014)	SUBICE Station #	Lat.	Long.	Modal Ice Thickness (m)	Mean Ice Thickness (m)	Mean Snow Depth (m)	Mean Ice Thickness at Bores (m)	Mean Freeboard at Bores	Mean Daily Air Temp. (C)
18 May	19	70.71	−166.28	0.8	0.88	0.15			−5.8
20 May	29	70.24	−163.25	0.8	0.79	0.09	1.09	0.09	−7.5
22 May	35	70.91	−164.99	0.7	0.76		1.04	0.09	−2.5
24 May	51	72.55	−166.39	1.1	1.13	0.18	1.45	0.12	−7.6
26 May	59	72.43	−168.30	0.9	0.92	0.15	1.42	0.10	−8.8
28 May	75	72.28	−162.42	0.7	0.76	0.12	0.89	0.08	−8.4
30 May	84	73.20	−161.96	1.4[a]	1.61[a]	0.15	1.46	0.12	−6.6
2 Jun	99	71.94	−166.33	1.0	1.07	0.28	1.19	0.06	−1.2
3 Jun	104[b]	71.58	−166.39	1.0[c]	0.99[c]	0.16	1.20	0.13	0.4
4 Jun	105[b]	71.67	−166.11	1.0[c]	0.99[c]	0.12	1.21	0.12	0.1
5 Jun	106[b]	71.66	−165.89	1.0[c]	0.99[c]	0.10	1.23	0.12	−0.3
6 Jun	107[b]	71.58	−165.82	1.0[c]	0.99[c]				−1.4
9 Jun	142	69.51	−168.70	0.8	0.86	0.04	0.66	0.05	−0.5
11 Jun	160	70.71	−168.31	0.8	0.92	0.07	1.40	0.12	−0.4
13 Jun	178	72.21	−167.48	0.8	0.92	0.13	1.04	0.09	−1.7
15 Jun	196[b]	71.36	−166.04	0.6	0.62	0.10	1.18	0.10	−1.4
17 Jun	209[b]	71.39	−165.34	0.6	0.74	0.04	1.09	0.12	−1.7

[a]Includes some MYI.
[b]Note that these sites all represent repeat visits to the same ice floe.
[c]Only one set of observations was collected, this is a four day occupation of a single floe.
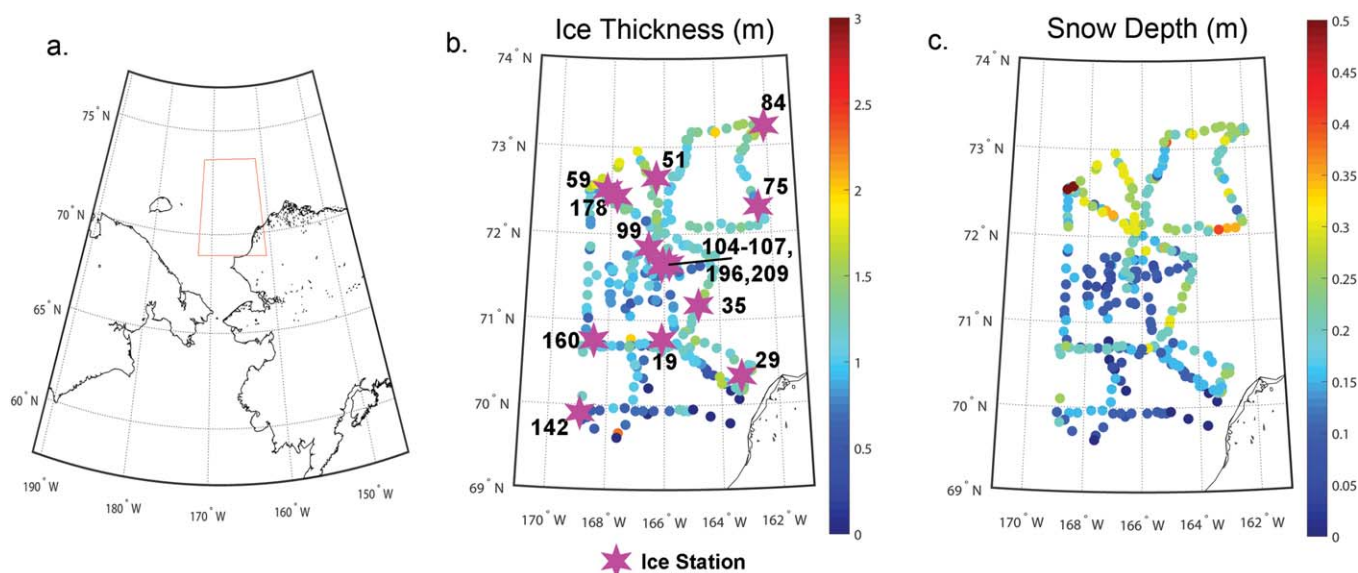
Figure 1. (a) Map of experimental region, (b) ice thickness observations, and (c) snow depth observations as observed every 2 h while underway according to the ASSIST protocol. Locations of ice stations are marked as magenta stars in Figure 1b, and labeled by SUBICE station number, as can be found in Table 1.

average or modal thickness of the floe by $\sim$0.25 m, indicating some apparent bias in site selection, though the sites were visually selected to be representative of the undeformed first year ice class on the floe.

Weather conditions in the region of our observations had a few notable features during May and June 2014. An isolated initial melt onset event occurred relatively early, prior to our arrival in the region on 18 May 2014. The melt event was recorded in the snowpack as a layer of refrozen melt grain clusters when we arrived and also detected by passive microwave sensors in early May (Miller and Markus, NSIDC Sea Ice News and Analysis, July 2014). This appears to represent a relatively early initial melt onset compared to the 1979–2013 mean, which is during the latter half of May across the sampled area [*Stroeve et al.*, 2014], though large variability in the date of initial melt onset is not uncommon. During the 18 May to 3 June, we observed temperatures ranging between −11°C and +1°C, in line with expected average conditions (e.g., 2000–2014 ERA-Interim reanalysis data), and minimal active surface melt between. A significant warm front arrived 3 June, near the average timing of sustained melt onset [*Stroeve et al.*, 2014], which again initiated surface melt across the area [*Stroeve et al.*, 2014]. As surface conditions warmed above freezing, however, a significant snowstorm occurred. The storm produced a total of $\sim$0.2 m of snow accumulation over the 3–6 June period, though ongoing melt during the accumulation period made cumulative measurement of accumulation challenging. We believe this snowfall had a strong impact on delaying the onset of sustained surface melt and hence ponding due to its impact on albedo, a matter for another paper. A colder period followed 4–16 June, with temperatures cycling in the range from −3 to +1°C, and remaining below freezing the majority of the time, preventing the onset of sustained melt. Pond formation did not begin in earnest until the time of our departure 17 June, and was not yet widespread as we left the area. Average (1979–2013) sustained melt onset date in the region is in the first week of June [*Stroeve et al.*, 2014]. Melt pond coverage retrieved from MODIS between 2000 and 2011indicates that pond formation typically also occurs within the first week of June in this region, and that ponds typically are well established by mid-June [*Rosel et al.*, 2012; MODIS Arctic melt pond cover fractions (v02), http://icdc.zmaw.de/]. We consider the conditions experienced by the ice we sampled in May to be not particularly unusual despite the initial early melt, given the large standard deviation in initial melt onset. We felt the delay in sustained melt onset was somewhat more unusual and, therefore, the observations we collected in mid-June represented ice that was in a somewhat unusually advanced state of internal melt for not yet having experienced ponding. As we discuss later in the paper, these June conditions would collectively represent a relatively prolonged or "slow" spring transition, with temperatures near the freezing point permitting the ice to warm and internally melt for an extended time prior to pond formation.
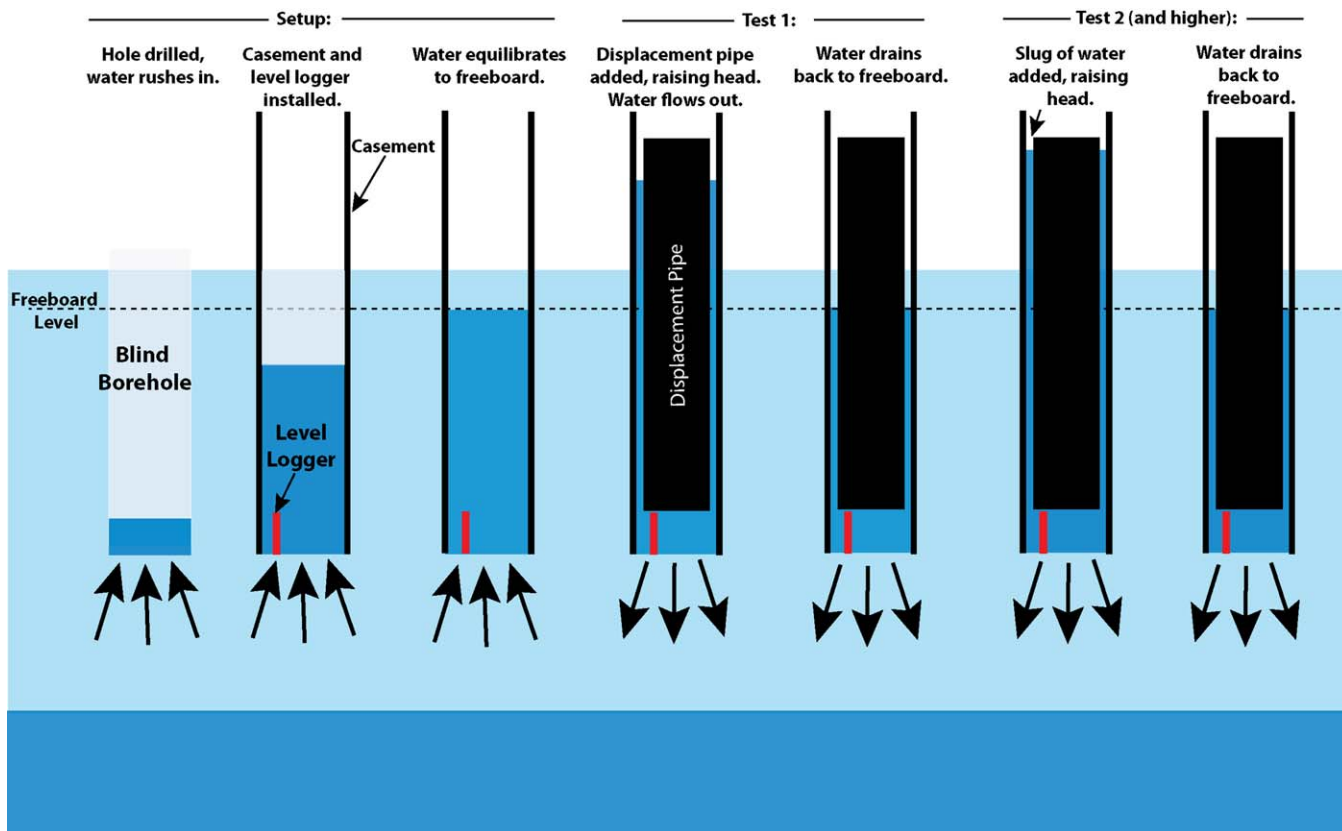
Figure 2. A schematic of the experimental apparatus used to test permeability of the sea ice. Light blue indicates sea ice, dark blue indicates ocean and water standing in the bore holes. (left) Borehole flooding during setup stages occurred quickly (<1 min). (middle) The addition of a displacement pipe raised the head and drove the same water that flowed during setup back out (Test 1) as a test of existing permeability. (right) Subsequent tests involved adding water, whose salinity was varied as an experimental factor.

2.2. Observing Permeability

Permeability tests were conducted by drilling boreholes partially through the ice using a 9 cm Kovacs corer (11 cm outside diameter) to establish a blind hole. Into this hole, we installed a borehole casing consisting of a 4" ABS pipe coated with closed cell foam rubber to seal against the entry of horizontal flow, similar to methods used by *Freitag and Eicken* [2003] (see Figure 2—Experimental setup for permeability measurements). A pressure-based water level logger, recording at 2 Hz, was placed in the bottom of the hole to record water level changes. The ice, even at the time of our first tests in May, was so porous, and inflow rates were so rapid, that the holes typically filled to near the sea level before the ∼ 45 s setup process could be completed. This confirmed our hypothesis that large porosity results in large permeability.

Due to the rapid flooding, a slug test was used to quantitatively determine the permeability, instead of monitoring inflow during the "bail test" imposed by core removal. The water in the casement was allowed to equilibrate at sea level, then additional water was added to the casement tube to raise the level above hydrostatic equilibrium and the rate of water drainage back to sea level was recorded. Conducting the test with positive hydraulic head permitted us to vary the salinity and temperature of the water entering the ice, mimicking conditions akin to having a melt pond forming over the ice. Evaluating how the salinity of intruding water alters permeability became a critical aspect of our experiment. At several sites, the water added in the slug tests was dyed with red food coloring to track how deeply it penetrated into the ice. To improve the sensitivity of the slug testing a 9 cm diameter sealed pipe section (see Figure 2) was installed within the casement in order to reduce the volume of standing water. This increased the ratio of pressure head to volume, so that a test of permeability could be completed with less water. The lower water throughput meant less opportunity for the pore structure of the ice to be altered by the test process. For tests where we changed the salinity of the slug test water, lower water throughput also enhanced our ability to understand precisely when our additions of water to the column had fully displaced the standing water in the bore and

begun entering the ice beneath. Added water needed only to displace the standing water in the annulus between the 9 cm outside diameter displacement pipe and 10 cm inside diameter of the casement pipe and around the pressure sensor at the bottom of the hole (see Figure 2). For a 30 cm deep bore, this allowed an addition of about 1000 mL of water to displace all water standing in the casement and for the test water to begin intruding into the ice. The addition of the displacement pipe also enabled us to evaluate the "pre-test" permeability from the first slug test in each hole. This test involved dropping the displacement pipe into the standing water in the bore, which immediately raised the hydraulic head and monitoring hydraulic head drop. The test minimized alteration of the existing porosity structure by displacing the very same water that rushed into the hole moments before and driving it back out, with the idea being to observe ice permeability prior to pore structure modification. Though some pore modification undoubtedly occurs, we expect the impact on permeability constant determined is minimal relative to spatial variability. We tested this expectation by conducting repeated tests at a two boreholes by adding and removing the displacement pipe (causing the same water to be forced in and out of the bore repeatedly). We found that permeability during eight such repeat tests (four repeats per bore) varied (increased) by <20%; far less than the variability between adjacent boreholes.

Boreholes for slug tests were mostly drilled to 0.3 m depth within the ice for comparisons of temperature and salinity impacts on permeability, though other depths within the ice column were used to test permeability in different parts of the ice. Depth is specifically noted during the discussion of results if other than 0.3 m. Few tests were attempted with boreholes of depth less than 0.3 m because the ice above this level was highly porous (estimated at 15− 25%+) and frangible, making sealing the borehole casing to the walls nearly impossible. Furthermore, the highly porous and frangible ice was readily ruled out as providing any barrier to water movement. Freeboard was typically between 10 and 15 cm, so the boreholes used in this paper all penetrated to below sea level.

We derive the intrinsic hydraulic conductivity of the sea ice from the slug tests following established methodology for conducting sea ice permeability tests [*Freitag and Eicken*, 2003]. The specific discharge, v, of fluid from the borehole (i.e., the vertical fluid velocity averaged over a horizontal cross sectional area) is related to the effective pressure gradient ∇p by Darcy's Law

$$v = \frac{-k}{\mu} \nabla p, \tag{1}$$

where k is the effective permeability of the porous medium in the vertical direction (described in more detail below), and μ is dynamic viscosity of water. Specific discharge can also be related to the change in hydraulic head in our tests according to the ratio between the tube cross section available for outflow (πr_o^2) and the tube cross section experiencing head change during the tests ($\pi r_o^2 - \pi r_i^2$), where r_o is the inside radius of the casement pipe and r_i is the outside radius of the inner sealed displacement pipe (see Figure 2). Since $r_o = 5$ cm and $r_i = 4.5$ cm, $v = 0.19 \frac{dh}{dt}$. The effective pressure gradient can likewise be related to the hydraulic head $h(t)$ through

$$\nabla p = \frac{g\rho}{L} h(t), \tag{2}$$

where g is the gravitational acceleration, ρ is the water density, and L is the thickness of the porous medium to be traversed, in this case ice. Substituting v and ∇p into equation (1) yields:

$$0.19 \frac{dh}{dt} = \frac{-k}{\mu} \frac{g\rho}{L} h(t), \tag{3}$$

$$\frac{1}{h(t)} \frac{dh}{dt} = \frac{-k}{0.19\mu} \frac{g\rho}{L}, \tag{4}$$

Integrating yields

$$\ln(h(t)) = \frac{-k}{0.19\mu} \frac{g\rho}{L} t, \tag{5}$$

or

$$h(t) = h(t_o) e^{-\frac{k}{0.19\mu}\frac{g\rho}{L}t}, \tag{6}$$

where $h(t_0)$ is the hydraulic head at time zero. Accordingly, fitting an exponential of the form $h(t) = h(t_o e^{-bt})$ to observed hydraulic head drop means that:

$$k = \frac{b\mu L}{0.19g\rho}, \tag{7}$$

where b is a constant fit to the data.

The permeability constant k represents the combined fluid loss in the vertical direction k_z and lateral directions k_x and k_y, as the plume widens beneath the hole. Since we are interested in k_z yet k_x and k_y are nonzero, we must take into account the fluid loss to lateral outflow. This is done assuming lateral permeability $k_x = k_y = 0.1k_z$ as in *Freitag and Eicken* [2003], resulting in a correction for k_z:

$$k_z = \frac{k}{0.17 + \frac{10.7}{L}}, \tag{8}$$

For each test then, k_z is determined by fitting an exponential curve to the pressure head time series. In cases where the water level returns to the original level, the best fit is required to return to zero hydraulic head. Tests that plug or do not fully drain, however, are not forced to zero.

2.3. Observing Ice Properties

Properties of the ice, including temperature, salinity, crystallography, and isotopic composition were observed. Data were collected from the ice that was removed to create the blind hole, and from the remainder core, removed from below the hole after the experiments were conducted. Additionally, a separate temperature and salinity core was collected nearby after each test to establish the full vertical profile of temperature and salinity prior to manipulation. Temperature was measured with a thermistor probe with accuracy ±0.1°C inserted into 3 mm diameter drill holes bored several centimeters into the ice. Salinity was measured by sectioning the core into 10 cm increments with a hand saw immediately upon removal and melting the 10 cm sections in sealed containers. Care was taken to minimize handling time in order to minimize brine leakage from the core. Meltwater salinity was measured with a YSI model 30 conductivity meter accurate to 0.1 PSU. Porosity is treated as equivalent to brine volume fraction, neglecting any entrapped air, and derived from these temperature and salinity measurements using the *Frankenstein and Garner* [1967] relationship,

$$p = S\left(0.0532 - \frac{4.919}{T}\right), \tag{9}$$

where S is salinity in PSU, T is temperature in °C, and p is brine volume fraction.

3. Results

3.1. Organization of Experiments

Our investigation into percolation blockage processes took the form of a series of experiments, which sought to explore particular aspects of the process by which infiltrating meltwater blocked permeability pathways in the ice. The experiments were, in practice, conducted in parallel. Some experiments were repeated at all sites to monitor temporal change, while others were targeted to address a particular process question and executed at only a subset of sites. Here, the results are organized by experimental topic, rather than site. We present the results in seven subsections, each demonstrating a particular aspect of the percolation blockage behavior. The intention is to address the questions a reader would have about the percolation blockage process sequentially, and not necessarily in the order the experiments were conducted. For the interested reader, Table 2 summarizes which experiments were conducted at each site, based on which sections of the results they support. These may be compared to site locations and conditions presented in Table 1.

The seven experiments are as follows. Section 3.2 presents results from tests that show permeability in unaltered ice, well prior to melt pond formation. This establishes the conundrum. As in prior experiments [*Polashenski et al.*, 2012], we observe that the ice is very permeable, but we know ponds will soon form above

Table 2. Experiments by Site

Date (2014)	SUBICE Station #	Baseline Permeability w/Porewater (Section 3.1)	Permeability With Varying Salinity (Sections 3.4, 3.6)	Dyed Water Borehole Tests (Section 3.4)	Δ bulk Properties (Section 3.5)	Volume of Water Required to Block (Section 3.7)	Permeability Versus Depth (Section 3.8)	Movement of Dye in Natural Pond (Section 3.8)
18 May	19							
20 May	29	X						
22 May	35	X	X				X	
24 May	51	X	X	X	X	X	X	
26 May	59	X	X	X	X		X	
28 May	75	X	X		X			
30 May	84	X	X	X				
2 Jun	99	X	X			X		
3 Jun	104[a]	X	X	X				
4 Jun	105[a]	X	X					
5 Jun	106[a]	X	X	X	X			
6 Jun	107[a]							
9 Jun	142	X	X					
11 Jun	160	X	X				X	
13 Jun	178	X	X				X	
15 Jun	196[a]	X	X				X	
17 Jun	209[a]	X	X				X	X

[a]Note that these sites all represent repeat visits to the same ice floe.

sea level on it. Section 3.3 demonstrates how infiltrating freshwater can rapidly block flow through permeable ice, showing a mechanism by which ponds can form on otherwise permeable ice. Section 3.4 uses experiments with dyed water to show where in the ice this rapid blockage of percolation occurs and demonstrate its morphology. Section 3.5 explores how the efficient blockage of connective pathways through the ice causes empirical relationships between permeability and porosity used in some sea ice models to break down. Section 3.6 seeks to better understand the dependency of permeability on intruding water salinity as the spring progresses, presents experimental results that vary the salinity of the intruding water. Section 3.7 uses two experiments where we varied the rate at which water increments were added to explore if the mechanism is governed by heat conduction rate. Finally, section 3.8 sets out to observe this process occurring in natural ice, not forced by the relatively large hydraulic gradients of our experiments. A schematic figure integrating the findings from these individual experiments into an overall understanding of this process is presented as Figure 13 in the discussion section. We refer to aspects of that figure supported by particular tests throughout the results section to help the reader integrate the findings. We place the actual figure, however, within the later section where it can be fully supported.

3.2. Ice Permeability

Permeability constant k_z is presented for each of our 63 individual borehole tests (small blue squares) and as a mean for each day of testing (large red squares) in Figure 3. Tests are plotted against (a) Julian date, (b) minimum porosity, and (c) minimum temperature in the ice remaining beneath the borehole. The results in this plot are calculated from the first slug test conducted in each borehole at the sites indicated in Table 2. Natural pore water that intruded into the bore as it was drilled is used as the fluid medium, as described in section 2. The tests were designed to capture the fluid permeability of the ice as near to its unaltered state as possible and are therefore suitable for intercomparison with prior works, which used intruding porewater as a test fluid [e.g., *Eicken et al.*, 2002; *Freitag and Eicken*, 2003].

A large degree of scatter in individual test results is apparent. Though the tests conducted at each site/day were all conducted in apparently identical thermodynamically grown first year ice, over an area not more than 20 × 20m, at a spacing of approximately 3–5 m, results typically indicate a permeability constant k_z varying over about one order of magnitude, with one site showing variability of three orders of magnitude. We attribute this large degree of variability to considerable heterogeneity in brine structures contained within the ice at the scale of these borehole tests [*Cole et al.*, 2004; *Cole and Shapiro*, 1998], and note that the variability observed is similar to that seen by prior authors using similar methods [e.g., *Freitag and Eicken*, 2003; *Eicken et al.*, 2002]. The possibility that even 3–7 tests do not yet cover sufficient area to capture the aggregate behavior of the ice seems likely. We find modest, but significant correlation between k_z and minimum ice temperature ($R^2 = 0.32$, $p = 0.003$). We find weaker and nonsignificant correlations
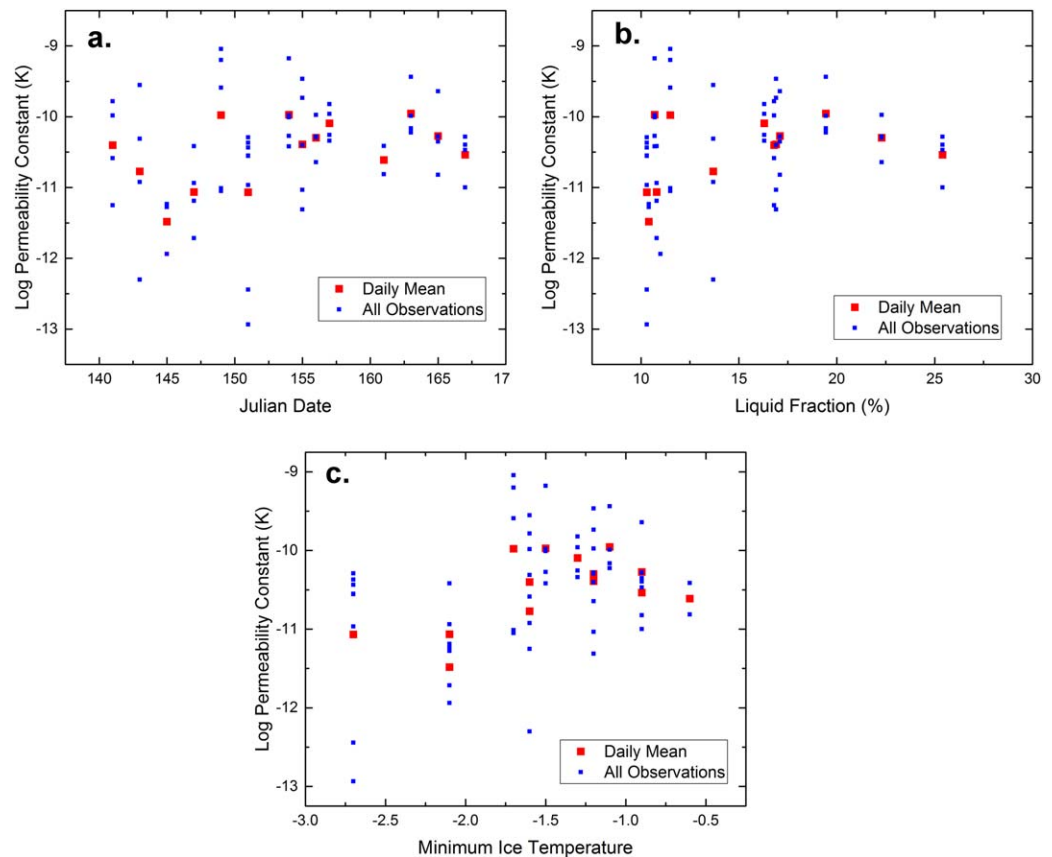
Figure 3. Upper ice permeability determined during the pore water flow test at each hole (Test 1 in Figure 1), plotted against (a) Julian date, (b) minimum ice porosity, and (c) minimum ice temperature. Large red symbols represent site averages, small blue symbols represent individual test holes.

between k_z and Julian date ($R^2 = 0.18$, $p = 0.063$) and between k_z and porosity ($R^2 = 0.15$, $p = 0.36$). Contributions from spatial variability as the ship moved between sites likely contributes to the poor correlation with Julian date. The data are consistent with a trend of greater permeability as the spring progression makes ice warmer and more porous, as expected, but indicates that other factors are also important, that our measurement technique captures considerable noise, or both.

The magnitude of the permeability constant determined is in agreement with prior works, so long as the timing of our observations is considered. Prior works focus on summer values after melt pond formation, while our observations cease at the time of pond formation. We expect the summer ice to exhibit higher permeability than spring ice. Our site-average k_z values increase from the range 5×10^{-12} to 9×10^{-12} m² in ice colder than $-2°C$, to 2×10^{-11} to 1×10^{-10} m² in warmer ice. The later range falls just below the range of early ponding season values observed a few weeks later in the seasonal progression by *Eicken et al.* [2002] (8×10^{-11} to 3×10^{-10}), suggesting a continuous trend in increasing permeability. Similarly, our "warm ice" permeability observations fall slightly below the *Freitag and Eicken* [2003] all-summer geometric means of 8×10^{-10} m² in 1995 and 4×10^{-10} m² in 1996, again indicating a continuation of the rise in permeability we observe. One notable difference is that our values suggest a smoother seasonal transition of permeability in spring than implied in *Eicken et al.* [2002, Figure 3]. There, a single early season test suggests an abrupt transition in first year ice permeability during the course of a week from below detection limits to $\sim 6 \times 10^{-11}$ m², a behavior we do not observe.

The most important point about the permeability values, however, is that all of the values observed are too great to permit the formation of above-sea-level ponds. Given hydraulic head of 1–10 cm and melt production rates of 1–3 cm/day on typical first year sea ice, the critical permeability constant, above which meltwater will not appreciably accumulate on the ice surface, is of the order 10^{-12} or 10^{-13} m² [*Freitag and Eicken*,

2003; *Polashenski et al.*, 2012]. The lowest permeability we observe is approximately 5×10^{-12} m^2, and at the time approaching pond formation all observations exceed 3×10^{-11} m^2. In other words, the multiday average permeability constant we observe in the days just prior to the onset of pond formation, 7×10^{-11} m^2, is sufficient to remove 30 cm of melt from the ice surface each day, given a hydraulic head of just 1cm. Under these conditions, ice must be considered highly permeable, with many connective pathways for water drainage (see Figure 13b), and pond formation above sea level seems improbable.

Many prior works [e.g., *Eicken et al.*, 2004] have found layers of superimposed ice forming on spring sea ice and suggested they may restrict fluid transport, enabling pond formation above sea level. We acknowledge that these layers certainly may be important to initial pond formation under some conditions, but note above that they are insufficient to explain observations of sustained ponding above sea level after the deterioration of superimposed ice layers [*Polashenski et al.*, 2012; *Landy et al.*, 2014]. Consideration of these layers here is important because superimposed ice layers would be missed by our observation techniques, which mostly examined permeability at 30 cm or deeper. Efforts to test layers shallower than 20 cm for impermeability typically failed due to obvious horizontal drainage. We were careful to note, however, that superimposed ice layers in this particular year were not widespread, likely due to thin snowpack (e.g., compared to observed in *Eicken et al.* [2002] or *Polashenski et al.* [2012]) and minimal early melt onsets prior to sustained melt. In all cases, including the few (5) individual bore sites where we noted a superimposed ice layer, the upper ice, including such layers, was highly deteriorated and visibly porous. Bulk temperature and salinity indicated liquid fraction of ~15% in the uppermost 30 cm of ice (see section 3.5) and we visually estimated total porosity typically exceeded 25% when air content was considered for layers having positive freeboard. These layers frequently fell apart when cored and only four times did core profiles yield ice layers that appeared could plausibly be locally impervious. We extracted segments of these and confirmed that they contained apertures permeable to fluids. Simply put, the upper ice was *highly porous* and we can confidently assert to the reader that no discrete impervious layer was present in the top few centimeters of ice that would have been missed by the design of our testing.

The observations that superimposed ice cover is heavily degraded either prior to pond formation or while ponds remain above sea level is in agreement with detailed sets of observations collected in both the Alaskan and Canadian Arctic. These found meltwater retention above sea level on ice with absent or noncontinuous superimposed ice cover [*Polashenski et al.*, 2012; *Landy et al.*, 2014]. Collectively this work and these prior observations demonstrate that a mechanism which restricts overall ice permeability both after a superimposed ice layer is compromised by melt and in conditions where widespread superimposed ice never formed must exist.

3.3. Demonstration of Permeability Blockage

It has been suggested that pond formation instead is enabled by percolation blockage occurring due to ice accretion within the interior of the ice [*Freitag and Eicken*, 2003; *Polashenski et al.*, 2012; *Landy et al.*, 2014]. *Polashenski et al.* [2012] provided theoretical and observational evidence that interactions between fresh meltwater and ice below the freshwater freezing point could block critical connective pathways as soon as percolation began, explaining the formation of above-sea-level ponds well after superimposed ice removal (see Figure 13c). Prior work had not, however, directly observed ice permeability. After confirming the discrepancy between observed permeability and formation behavior of melt ponds, we set out to demonstrate and explore the interposed ice formation process.

Results showing hydraulic head drop versus time for a typical borehole drainage experiment from prior to the onset of sustained melt are shown in Figure 4. The test, conducted 26 May 2014, consisted of a pair of boreholes 30 cm deep, positioned approximately 3.5 m apart, in a sheet of homogeneous, level, thermodynamically formed first year ice 1.19 m thick. The curves represent water level in the hole over time after each addition of a 750 mL increment of water. The minimum temperature in the ice column at the time of this test was −2.1°C at a salinity of 4.5 PSU, corresponding to a brine concentration of 41 PSU and a brine volume fraction of 11%.

Based on the ice properties, we expected that the ice would be permeable and that, upon intrusion, water would rapidly drain. We further hypothesized that, if the percolation blockage mechanism was valid, water fresher than 41 PSU would accrete ice within pore space as interposed ice, restricting flow over time, while water more saline than 41 PSU would erode and enlarge the pore space, enhancing flow. To test these
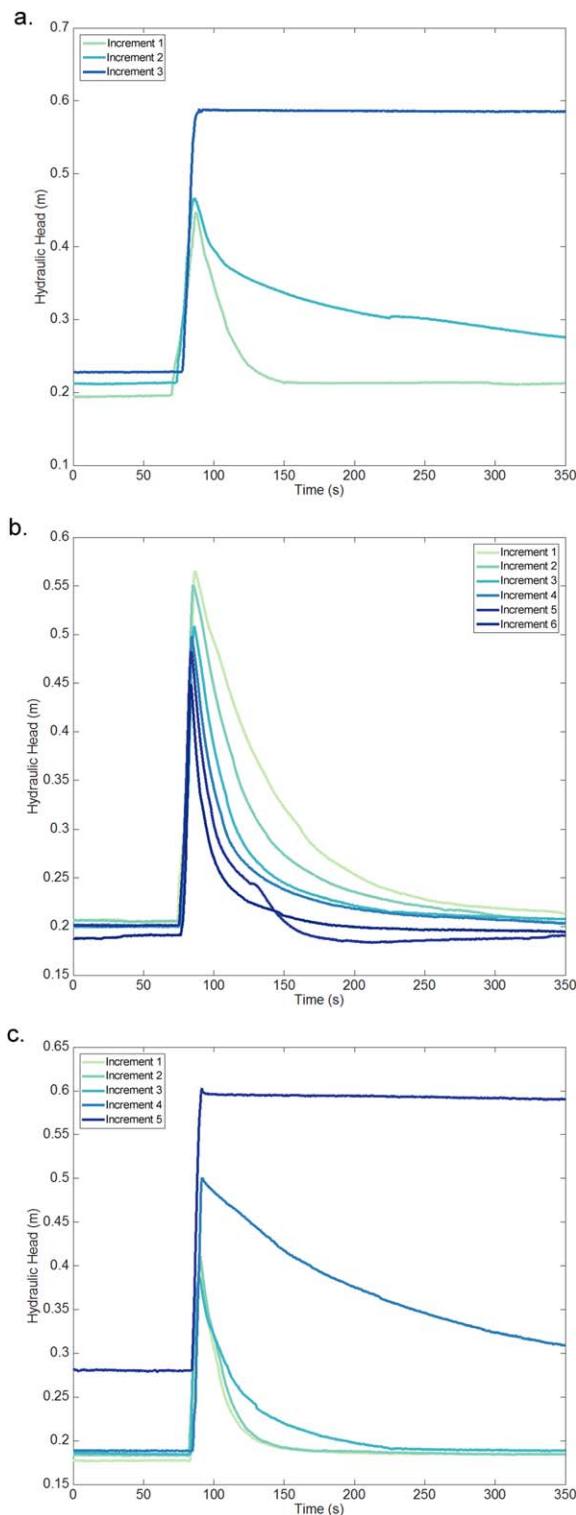
Figure 4. (a) Plot of hydraulic head versus time for multiple additions of 750 mL increments of 0.3 PSU water at its freezing point, conducted 26 May 2014. Note that only three increments of water are possible before no more drainage occurs. (b) Plot of hydraulic head versus time for multiple additions of 750 mL increments of 57 PSU water at its freezing point, conducted 26 May 2014. Note that each subsequent test in the same hole results in an acceleration of drainage. An increase in drainage rate during test 5 may represent the formation or enlargement of a new connective pathway. (c) Plot of hydraulic head versus time, for fresh water added to the borehole used in experiment (b), after the saline water addition tests were complete. Despite the enlargement of the connective drainage pathways, the freshwater still rapidly blocks percolation.

hypothesized impacts on percolation, we added water with a salinity of 57 PSU to one borehole and water with salinity 0.3 PSU to the other. In both cases, the water was added at its salinity-determined freezing point, $-2.9°C$ and $0.0°C$, respectively.

The hydraulic head in both tests initially drops exponentially as water percolates into the ice through the open bottom of the casement tube. The hydraulic head approaches the original level within minutes (Figures 4a and 4b). As expected from theory, this indicates the ice is highly permeable at this time of year, prior to the formation of ponds. After each subsequent addition of water, the hydraulic head in the high salinity test case drops faster than in the test before, indicating that the cold, saline water is eroding the microstructure of the ice and enhancing the flow pathways. In contrast, subsequent additions of fresh water slow, and then block, percolation (Figure 4b). The first one and a half additions of 750 mL increments of freshwater behave in a similar manner to the saline water tests, because this volume of fresh water displaces the saline pore water standing in the casement from prior to the test. Once the standing water in the casement (~1000 ml) has been displaced and fresh water begins to enter the cold ice pore structure, the rate of hydraulic head decline slows, and soon drainage ceases altogether. The percolation pathways appear to have been completely blocked, and the blockage remained in place for at least several hours at which time we had to leave the site.

We conducted more than 20 similar tests, including at least one at each site, in order to rule out the possibility that spatial variability in pore structure, rather than salinity of water added, caused the divergent percolation behavior. In all cases, either only the freshwater case blocked percolation or neither test did. Cases where freshwater did not block percolation occur only at four sites that were sampled later in the seasonal evolution, when ice temperatures are greater. These are discussed further in section 3.5. At four sites we also added fresh ($\leq$ 0.3 PSU) water to the high salinity borehole after completing a series of high salinity percolation tests. Despite the improved network of brine pathways created during the high salinity experiments, the fresh water still blocked percolation in the hole during six of the seven such tests. One such test is shown in Figure 4c. Fresh water is added to the same borehole whose tests are shown in Figure 4a, immediately after the last high salinity test shown, resulting in percolation blockage. The result indicates the water salinity is a more important factor than spatial variability in pore structure and that fresh water can block even relatively enlarged pore structures, so long as the ice remains cold enough to refreeze the water and sufficient fresh water is available.

3.4. Examining the Location of Permeability Blockage

We hypothesized that percolation blockage in the freshwater case was occurring because ice accreted deep within the microstructure of the sea ice, blocking connective pathways (interposed ice formation), rather than on or near the ice surface at the bottom of the borehole. We formed this hypothesis because we observed warm and highly porous ice at the immediate bottom of the borehole, and because we did not observe any discrete ice layer formation at the bottom of the borehole after tests resulting in percolation blockage. In order to evaluate this hypothesis, we conducted 1–3 borehole tests using fresh water dyed with red food coloring during experiments conducted 24, 26, 30 May 3 and 5 June. After each test, we extracted the ice beneath the boreholes in a core for examination and found similar results. Photographs of a representative remainder core, in this case from a test conducted on 5 June beneath a 30 cm bore, are shown in Figure 5. The dye indicates where water reached during the test. The test began with large drainage rates, and concluded with zero drainage at hydraulic head of some 0.4 m, equivalent to the test shown in Figure 4b. Three aspects of the dye distribution are notable. First, the dye saturates the upper and extreme lower ice, indicating free movement to nearly all pore space where porosities are large. Second, the dye percolated through the entire thickness of the ice indicating that connective pathways to the ocean were present and some dyed water followed these before blockage occurred. Indeed, a significant volume of dye apparently penetrated the ice interior, based on dye saturation of the lower ice near contact with the ocean where higher porosity and pore connectivity enabled the dye to spread out again. Third, the dye traveled through only a very few connective pathways in the colder, interior portion of the ice. Much of the liquid brine in this interior section of the ice was contained in isolated chambers not along these connective pathways and therefore was not replaced by dyed liquid. Close examination of core cross sections in the field confirmed that the dyed water in the interior of the ice had completely frozen where it had traveled in isolated channels, demonstrating the formation of interposed ice as a percolation blockage mechanism under experimental conditions (see placement of ice plugs in Figure 13c).
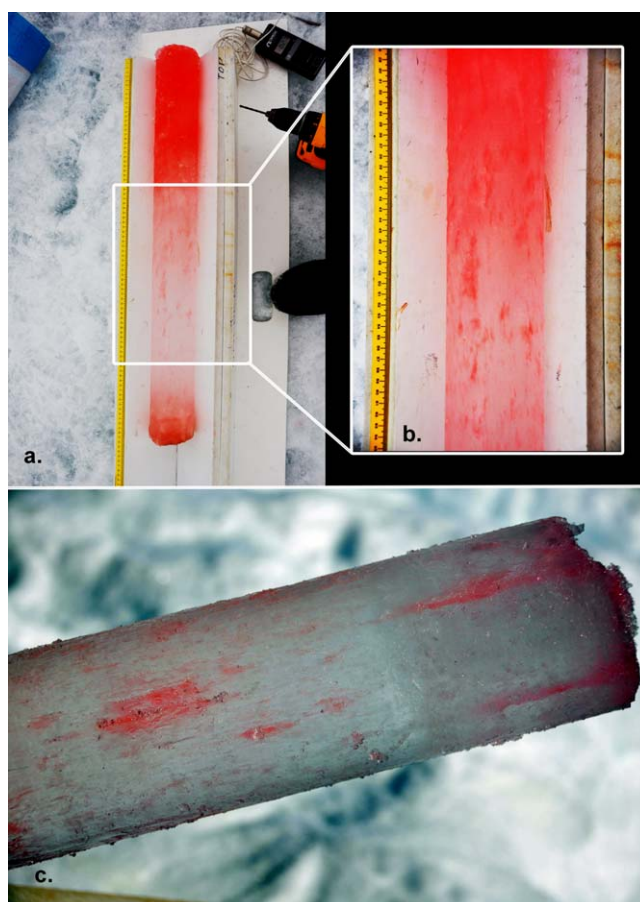
Figure 5. Saturation-enhanced photos of red dyed core showing penetration of fresh water in to sea ice 5 June 2014. Note in close up images (b) and (c) that dye has penetrated along a small number of connective pathways in the ice interior rather than through the bulk of the ice.

3.5. Testing Impact of Interposed Ice Formation on Bulk Permeability-Porosity Relationships

We measured the salinity and temperature profile of the ice before and after percolation tests conducted 24, 26, 28 May and 5 June. Bulk salinity and temperature results are plotted in Figures 6a and 6b, along with bulk porosity of those sections (Figure 6c), as derived from the *Frankenstein and Garner* [1967] relationship. The "pre-test" properties (black) were evaluated from ice cores taken several meters from the borehole tests. The posttest properties (red and blue) were evaluated from the ice beneath the borehole after the test. Salinity data from individual cores tend to be noisy, making comparison of a particular before/after case challenging due to spatial variability. Here we average the data from the four tests, such that the profiles presented for the different test types each represent the average of four core profiles, one core per site. The results indicate little change in the ice's bulk properties during the test, and particularly that bulk porosity remains well-above expected percolation thresholds of 5% or even 10% after the tests. This is an important observation because prior literature on sea ice permeability has established relationships between

porosity and permeability of the ice [i.e., *Golden et al.*, 1998, 2007] which are increasingly being incorporated into model parameterizations [*Hunke et al.*, 2015]. The observation that bulk porosity did not drop below expected percolation thresholds and yet the ice became impermeable indicates that the sea ice deviated from these relationships. The implication is that the sea ice does not obey established porosity-permeability relationships after the intrusion of fresh water. We hypothesize that this deviation is caused by the intruding water being preferentially directed into the critical connective pathways through the ice interior. There it freezes and blocks percolation with minimal impact on overall salinity. Ice accretion in the critical pathways, therefore, preferentially blocks connective pores and alters the fundamental assumptions of random pore geometry distribution upon which statistically based porosity-permeability relationships are dependent (see blockage in Figure 13c). The dye experiment in Figure 5 shows an ice accretion pattern that supports this hypothesis.

A simple energy balance can further confirm that alteration of the bulk porosity to levels below the percolation threshold would simply not be possible. The available specific heat capacity of 1 kg of ice at −2.1°C is only sufficient to take up the latent heat release from about 10 g of new ice formation—capping the porosity change due to refreezing fresh water in pore space at around 1%. Ice in the interior of the dye experiment core, like most of our tests, had porosity levels of 10–15%, fully 5–10% above the permeability threshold. Thus, the fresh water did not block percolation by altering bulk porosity sufficiently to cross established percolation thresholds. Rather it sealed the ice by forming plugs in critical pathways (see Figure 13c), altering the "random" pore space geometry upon which statistically based porosity-permeability relationships depend.
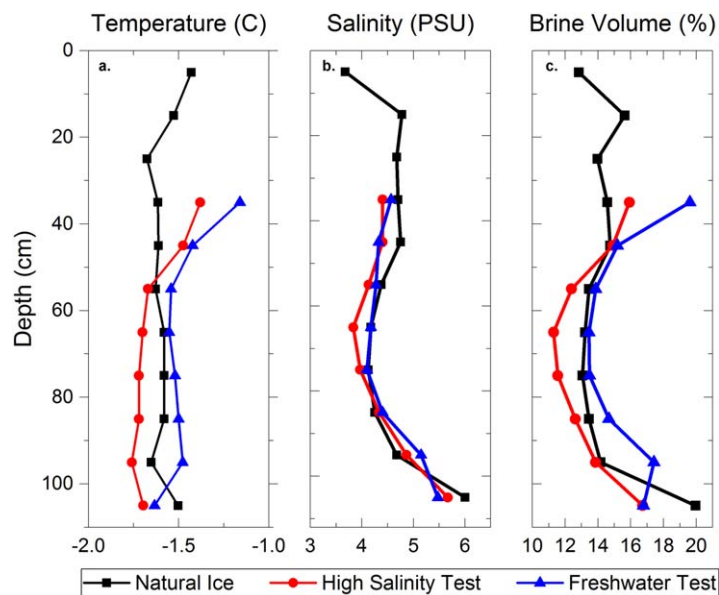
Figure 6. Properties of the ice before and after conducting percolation tests. Panes from left to right are (a) temperature, (b) bulk salinity, and (c) derived bulk porosity [*Frankenstein and Garner*, 1967]. Natural ice (black) properties are observed several meters from the test site in the same ice type, to represent a "before" case. High salinity (red) and freshwater test (blue) properties are determined from coring ice beneath the test boreholes after test completion. Data are an average of four tests conducted 24, 26, 28 May, and 5 June 2014.

3.6. Seasonal Evolution of Salinity Dependence in Blocking Behavior

The tests shown in Figure 4 demonstrate the ability of pure fresh water to block percolation under experimental conditions. Observations made in the field, however, indicate that pore water salinity varies. The pore water did not become entirely fresh, even later in the melt season when appreciable snow-melt flushing was occurring. We therefore conducted tests to understand how water of varying salinity interacts with the ice as the ice warms during the spring. Using these tests, we attempted to bracket the "critical salinity"—the value below which the intruding meltwater will block percolation and above which percolation proceeds freely. Results of these tests were typically con-clusive and binary. Either the hole blocked before the addition of the fourth or fifth increment of water or it did not at any point. The size of the range between tests bracketing the critical salinity was therefore dictated by time and equipment constraints limiting the number of tests available, not by ambiguity in test results.

The results of this experiment series are shown in Figure 7. For each day that tests were conducted, we plot the highest salinity tested that still blocked permeability and the lowest salinity tested that did not. The blue curve indicates the salinity of water that would be in equilibrium with the lowest temperature observed in the ice. When water at salinity below this "equilibrium line" percolates into the ice interior, at least some ice accretion is expected within the pore space from intruding water. We find that the critical salinity range we bracket initially includes the "equilibrium line." Later, however, there is a transition to needing water fresher than would be in equilibrium with the coldest layer of the ice in order to block perco-lation. Still later, on 13 and 15 June, only fully fresh 0 PSU water blocked percolation and tests became inconclusive. Many (10+) additions of fresh water over periods of several hours were required to produce blockage in some holes, while fresh water did not block other boreholes at all. (Hence symbols for both bracket points placed at 0 salinity.) By 17 June, no tests, even with 0 PSU water were able to block percola-tion. We interpret this evolution—from bracketing the equilibrium line, to dropping below it, to no longer being able to block percolation at all—to internal melt and the enlargement of pore size (see transition between Figures 13c and 13d), which is a function of ice temperature.

Modeling in *Polashenski et al.* [2012], used to discuss the impact that the size of a connective pathway has on the ability for ice accretion to block it, can be applied to support this logic. *Polashenski et al.* [2012] used a model of a single idealized brine channel with intruding meltwater to demonstrate the concept of a criti-cal flaw size. In ice of a given temperature, the critical size is the flaw diameter above which the surrounding ice does not have sufficient specific heat capacity near enough to the flaw to remove the latent heat depos-ited by ice accretion before the meltwater can begin to erode the ice. *Polashenski et al.* [2012] focused on understanding how flaws can enlarge to form meter-scale meltwater drainage pathways when initiated above the critical size. In our tests, which successfully block percolation, we are dealing with pore structures that are all below the critical size. Presumably, as the pore structures enlarge with ice warming the pore size approaches the critical size. Figure 8, reproduced from *Polashenski et al.* [2012], shows the model results pre-dicting how the diameter of an idealized channel through the ice changes over time when freshwater
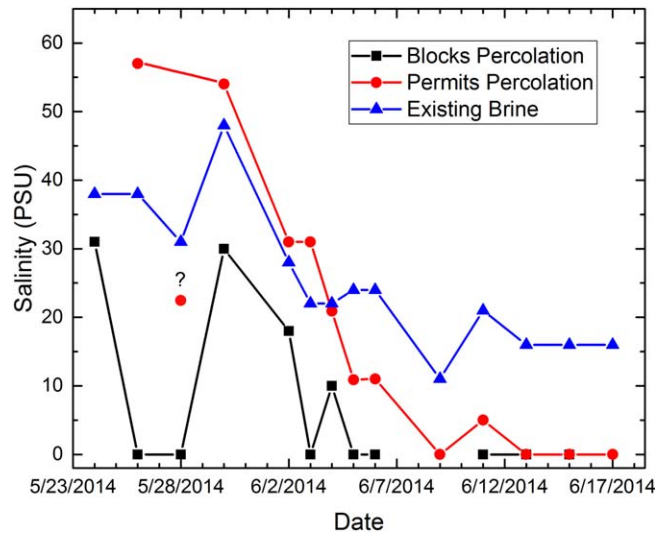
Figure 7. (black) Results of variable salinity slug tests, showing the maximum water concentration tested which blocked percolation and (red) the minimum concentration tested which permitted percolation. (blue) Also shown is the brine salinity in equilibrium with the coldest temperature in the ice. An outlying test on 28 May, labeled with a question mark, was conducted in a floe with no snow pack that exhibited very high porosity. This is the floe discussed in section 4.2 under the first paragraph of the section *Snowpack Water Content* and is thought to represent an alternate pathway where sea ice with low snow cover may become highly porous and unable to support above sea level ponding.

intrudes. As ice warms and pore space enlarges due to internal ice melt, pores interacting with meltwater follow paths that begin from larger initial pore diameters (up the *y* axis). Model results show that blocking these larger holes takes more time, with a given salinity of water, than does blocking smaller holes. Percolation tests, therefore, should take longer and longer to reseal growing pore structures as the spring evolution occurs, until the flaws in the ice pass a critical size (or the ice warms too much).

We reason that this mechanism explains why the critical salinity required to block percolation eventually drops below the salinity of water whose freezing point is in equilibrium with the coldest temperature in the ice. As the pore size increases, the formation of an ice plug that blocks a pore requires the removal of greater amounts of latent heat due to larger amounts of ice formation. Greater temperature gradients and more time are required to transport this heat away from the freezing site. Water fresher than the equilibrium salinity can aid this heat removal by freezing at a warmer temperature. The higher freezing point increases the effective available heat capacity of the surrounding ice and increases the temperature gradients available for conduction, helping to block larger flaws. The enhancement in freezing provided by fresher-than-equilibrium water permits ice accretion to block large pores for a time, until the typical pore size is simply too large and the ice is simply too warm for the remaining heat capacity to freeze intruding meltwater completely. Ice begins accreting on the walls of a connective pore, but there is not enough remaining heat capacity to cause blockage (see Figures 13c and 13d).
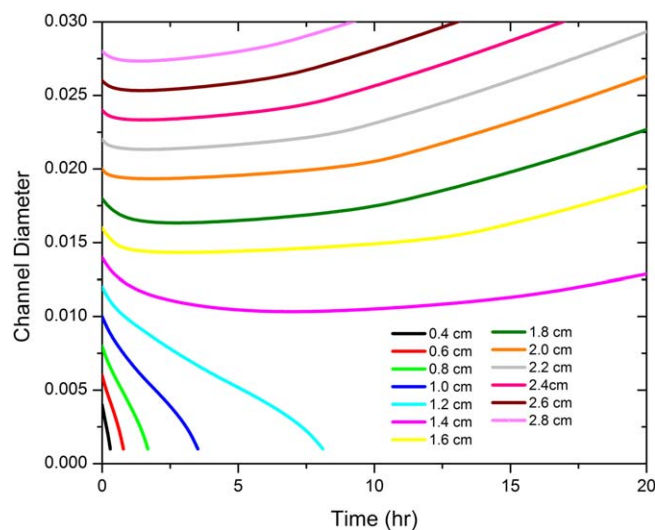
3.7. Time Dependence of Blockage Behavior

We recognize that our tests of water percolation were likely driving larger volumes of water into the ice structure more quickly than would occur during natural meltwater percolation. Still, by varying the addition rate, and examining the response behavior, we hypothesized, would show whether blockage was primarily contact limited or heat conduction limited (as hypothesized for large channels in 3.6). In a contact-limited case, water would need to penetrate to some depth within the ice by displacing pore water, but then would block percolation quickly when it contacted cold ice in a small pore—the time required for heat conduction would

Figure 8. Results from a model of percolation blockage in an idealized brine channel, originally presented in *Polashenski et al.* [2012]. The results show the time required for blocking a pore increases as the channel size approaches the critical value.

be negligible. In a conduction-limited case, water would need to spend time in contact with cold ice to create a frozen plug because heat removal (conduction) into the surrounding ice would be the limiting factor.

We therefore conducted additional tests to determine if blockage was dependent on the volume of water flushed through the ice or simply on the time elapsed since fresh water had entered an appropriate point in the pore space. The tests involved adding increments of fresh water at different rates. On two occasions, 24 May and 2 June, we installed several casements in identical bore holes in apparently homogeneous, level, thermodynamically formed first year ice. Water was added to the bores in 750 mL increments at intervals of 0.5, 2, and 5 min during the three 24 May tests and 0.5, 2, 5, 10, and 15 min during the five 2 June tests, respectively. Approximately 1000 mL of pore water is present in the casement at the start of the test, so all of the first and part of the second increment of water was required to displace the standing porewater in the tube and begin pushing freshwater into the ice beneath.

During the first test, the ice remained relatively cold, with a minimum internal temperature of $-2.2°C$. In this case, we found that all test bores exhibited percolation blockage after the third water increment was added. The fact that a *third* increment of fresh water was needed indicated that meltwater needed to percolate to some depth before blockage occurred, because casement water is fully displaced and approximately 500 mL of test water (an equivalent of ~ 5 cm snow water equivalent) is pushed into the ice matrix by the second increment of water to our apparatus. Blockage did not occur after this second increment in any test. Since the uppermost ice was below the freezing point of fresh water, we interpreted this to mean that, though ice likely accreted in the pore space of these upper ice layers, the pores were too large and too connective to be blocked. Insufficient specific heat capacity remained for freezing (see upper ice in Figure 13c). The observation that all test bores blocked during the drainage of the third test, regardless of increment addition rate, indicated that all tests were driving water into the ice slowly relative to the rapid freezing process and the process was contact-limited. Pores within the colder ice layers were completely blocked within 30 s of fresh water reaching them. The connective pores were small and surrounded by cold ice. The observation that a volume of water greater than required to displace the standing water in the test tube was required to initiate blockage suggested a significant amount of fresh water may be required to initiate percolation blockage. In our case the amount was equivalent to 5 cm of water or about 15 cm of snow at typical densities—this would represent all of a low, but not unusual, snowpack on first year ice compared to observations in Barrow (see Figure 14a).

During the second test, the ice was warmer and more porous, with a minimum internal temperature of $-1.5°C$. In this case, we found that all holes exhibited blockage after *at least* three water increments were added. This time however, approximately 5 min elapsed before blockage, even though additional increments of water were added and passed through the ice in the rapid-addition cases. This indicated that the time required for blockage under these conditions was nearly constant regardless of inflow rate. The large quantities of water added in the faster tests were not required for blockage. Freshwater simply had to be forced into the ice to sufficient depth to come into contact with cold ice, and sufficient time had to elapse for heat conduction to remove latent heat, freezing enough ice to block the pore space. In this case, the critically connective pores were apparently large enough that several minutes of heat conduction were required to remove the latent heat deposited by the freezing water.

We are not certain what a typical rate of meltwater injection into pore space is in a natural environment, but expect it varies widely. A newly opened flaw at the bottom of an above-sea-level pond, created due to internal melt, may experience high injection rates and pressures, similar to those we test. Initial contact of snowmelt with the ice surface in early melt would be expected to occur at far slower rates and with negligible pressure. We conjecture that in the course of a seasonal evolution the injection of freshwater proceeds very slowly at first, with little water available and ample time for conduction to remove heat from refreezing water deep into the ice. This would encourage most reforming ice to form at or near the surface (i.e., superimposed ice). As sustained melt onset occurs, more rapid melt rates could create as much as a few centimeters of liquid water at a location with 10+ cm of positive hydraulic head in a matter of hours—potentially overwhelming vertical heat conduction and driving water into the upper ice at a moderate pace. Still later, water sitting on the ice surface in a typical early season FYI pond, which is on the order of 10 cm above sea level, has the capability to inject large amounts of water rapidly and forcibly into any flaw that should become newly connective due to internal ice melt or the removal of a superimposed ice layer. Our tests may be reasonably representative of this latter process.

It would be natural to hypothesize that slower additions of smaller increments of water than were tested might have produced blockage higher in the ice column, by giving time for vertical heat conduction to occur. Too much pore space was present in the uppermost ice layers, however, to be refrozen without atmospheric driven cooling. It is likely that temperature-salinity interactions between sea ice and meltwater in nature operate along the full continuum with a shift from producing more superimposed ice and interposed ice of large volumes near the surface early in the melt season to producing exclusively interposed ice deep in the ice interior later. In the next section we seek to observe the later, production of interposed ice after vertical temperature gradients are largely absent and superimposed ice production is no longer feasible, in natural conditions.

3.8. Percolation Blockage in the Real World

With these experiments demonstrating the important role intruding water likely plays in controlling ice permeability under experimental conditions, we attempted to observe the natural occurrence of percolation blockage during the onset stages of melt pond formation. Two experiments were performed for this purpose. The first involved repeatedly testing the permeability of the sea ice at different levels as fresh water was observed naturally flushing brine from the ice. We hypothesized, incorrectly, that this test would show permeability dropping to zero in certain layers of the ice after fresh water had the opportunity to naturally intrude. We reasoned this because we assumed blockage would occur at a uniform depth in a discrete layer as percolation water encountered ice of a particular temperature. We did not, however, find such a layer. The second test involved covering an area of ponded ice with dye to trace movement of pond water, then perturbing the pond bottom to examine the impact on brine movement. This more clearly showed the nature of the process.

To conduct the first experiment, several times prior to generation of appreciable melt (22, 24, and 26 May) and during the melt but prior to significant pond formation (11, 13, 15, 17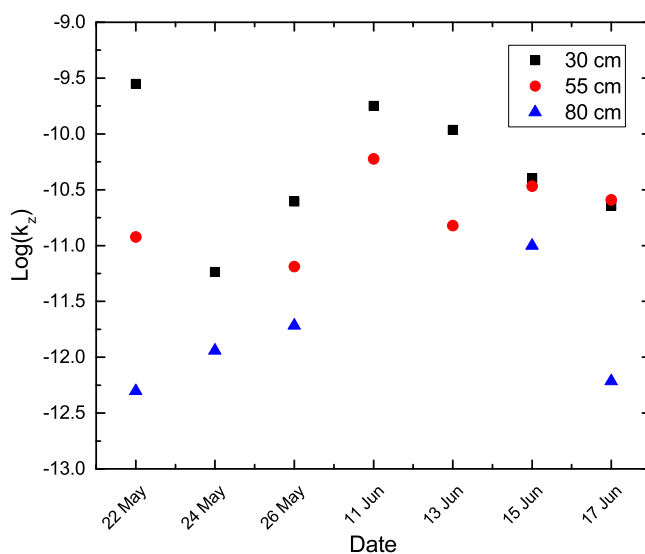 June), we drilled three boreholes to nominal depths of 30, 55, and 80 cm, installed a casement tube in each, and conducted slug tests to assess permeability. We used the intruded pore water as the test fluid to avoid changing the ice structure, accomplishing the slug tests by the addition of a displacement pipe as described in the methods section. A plot of the derived ice permeability versus date at each depth is presented in Figure 9 for these tests. Site to site variability dominates, though later season (11–17 June) observations indicate a statistically significant ($p = 0.048$) increase in permeability compared to earlier season (22–26 May) observations. Permeability is lower in deeper boreholes in each case, as expected from the lower temperatures at these depths. At no point, however, do we find evidence of a discrete, fully impermeable layer within the ice. In all tests, water percolates rapidly through the ice at all depths tested. Though such a layer would have been missed by our tests if it had existed above our shallowest test (30 cm), as we note in section 3.2, we were able to confirm that the ice above that depth was highly
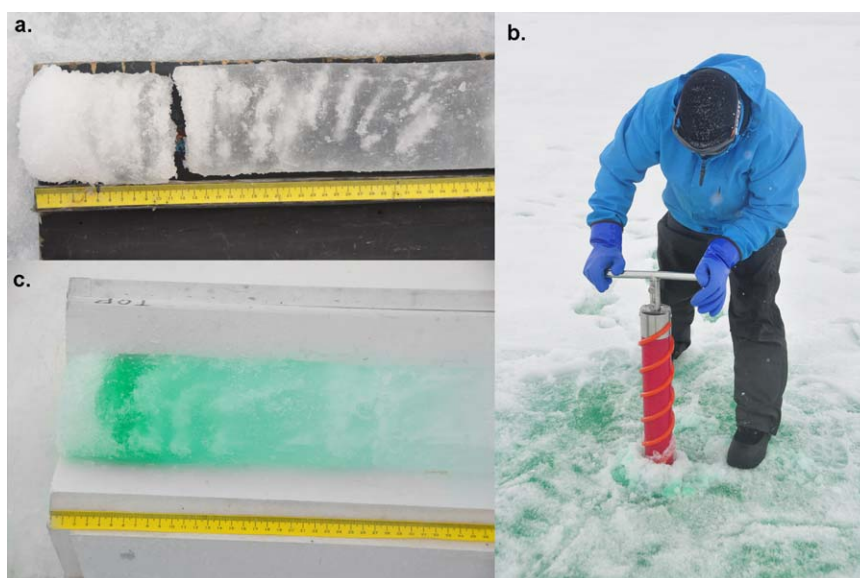

Figure 9. A plot of the log of derived ice permeability constant, k_z, determined at three nominal depths, presented by date. Note that x axis is abridged between 26 May and 11 June. All of the bores exhibited finite permeability, and there is no layer with apparently zero permeability. Missing values represent tests that were not undertaken. Shallower bores show greater permeability in general. There are indications that permeability is increasing with time, despite significant scatter. $Log(K_z)$ in the latter interval (11–17 June) averages -10.60, 0.58 greater than in the earlier interval (-11.18, 22–26 May), and the increase is significant at the $p = 0.05$ level (0.048). The 17 June 80 cm depth test was noted as an outlier at the time it was collected—no other observations of permeability so low were recorded late in the season. It is possible that this test was drilled into deformed ice (i.e., a block turned on its side). Unfortunately, we did not retain the core for analysis. Discarding it appreciably increases the difference between the two groups (0.75) and statistical significance level ($p = 0.018$).

Figure 10. (a) Photo of a typical core immediately after extraction showing rapid brine drainage throughout the uppermost 30 cm, (b) coring from an area where dye had been spread on the ice surface, and (c) the core extracted in Figure 10b showing dye penetration well into the upper ice layers.

degraded and extremely unlikely to be impermeable at all test holes. Shallower tests of permeability were not conducted because the ice was so rotten it was impossible to seal the boreholes we attempted in the upper 30 cm of the ice against lateral outflow. A photo of a typical upper ice core taken 7 June, immediately ($<$10 s) after extraction, is presented in Figure 10a, documenting this high porosity. The brine has completely drained from the uppermost $\sim$10 cm the ice, giving it a white appearance, and white spots are already appearing throughout the upper 30 cm of the ice indicating rapid brine drainage from well-developed porosity. On 5 June, dye was also placed on the ice surface, permitted to soak in, and a core was later extracted (Figure 10b). A photo of this core (Figure 10c) shows that the dye readily spread throughout the upper ice prior to extraction, again indicating free water movement in these upper ice layers.

We also observed the salinity of upper ice pore water during each test to determine whether the fresh water we expected to be intruding into the ice from the observed snowmelt actually was intruding. We found a pronounced freshening of the upper pore space water at the onset of melt. Pore water intruding into bores 30 cm deep transitioned from over 35 PSU to less than 7 PSU between 2 June and 6 June, indicating that the fresh water necessary for pore space blockage was available and percolating into the ice (as illustrated by pore space water shading in Figure 13c). Such a pore water freshening could have been caused by flushing that physically removed salt from the upper ice or by dilution of the brine with surrounding ice melt. Bulk salinity observations, averaged to smooth site to site variability (Figure 11), show that salt was actually being flushed from the upper ice during this time, consistent with prior observations [*Polashenski et al.*, 2012; *Landy et al.*, 2014], and indicating that fresh water was indeed penetrating down into the ice interior.

Despite our inability to locate a discrete impermeable layer, melt ponds forming at the end of our observation period (17 June) were found to be well above sea level, requiring ice permeability of less than 10^{-12} in the ice beneath them (a scenario similar to Figure 13c, without the extra large flaw that cannot be blocked). To investigate these ponds, we dyed the water of a melt pond during these early formation stages and tracked the dye movement in a pond instrumented with a level logger. Green food coloring dye was added to an above-sea-level melt pond, which was mostly between 13 and 19 cm deep on 17 June 2014, and a level logger was installed to track pond level. After a period of 2.5 h, partial cores were removed from the bottom of the melt pond to depths of 31, 45, 61, and 81 cm, of a total ice thickness of 109 cm. Each of these partial cores exhibited dye penetration 15–25 cm into the ice beneath the pond. The rapid dye penetration well into the ice was consistent with our observation that the upper layers of ice at the pond bottom were highly deteriorated and did not appear to be covered by a layer of superimposed ice. Brine fractions of as
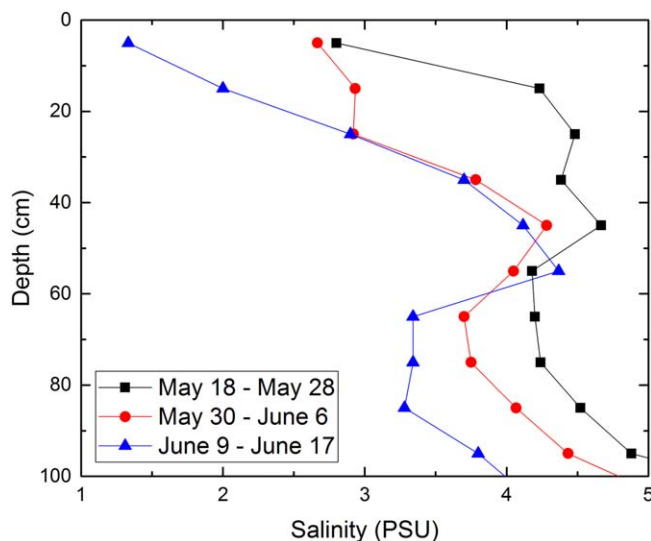
Figure 11. Desalination of the upper ice. Each curve represents the average of six salinity observations (1 per site) collected during the time interval indicated in the legend. Note the desalination of the upper ice, indicating salinity flushing, and near-static salinity of the ice interior from 40 to 60 cm. This plot indicates desalination behavior very similar to that presented by *Polashenski et al.* [2012] and *Landy et al.* [2014].
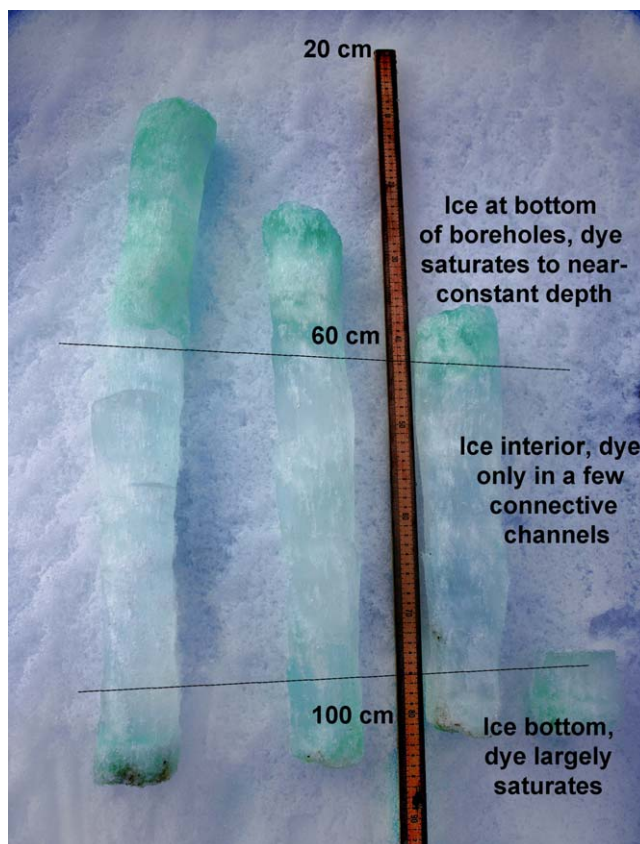

Figure 12. Contrast enhanced image of cores removed from melt pond bottom. Note high dye concentrations in the upper part and lowermost parts of each remainder core, where porosity is high, while the cold interior of the ice has very limited dye concentration, only in discrete paths. Labels next to scale ruler indicate depth from original surface.

much as 40% in these upper ice layers permitted easy water movement and/or mixing. The dye movement appeared to be caused by the greater density dye freely settling into connective structures in the rotten upper layers of the ice and not due to water drainage. The pond level logger recorded less than 0.25 cm change and, since slightly below-freezing temperatures prevailed, minimal melt inflows were expected.

Two hours after drilling the partial boreholes in the pond bottom, we revisited the pond. Air temperatures remained very near or below freezing and we expected minimal inflow. Water level in the pond had dropped approximately 0.75 cm, indicating some outflow had occurred. We cored out the remaining ice at the bottom of the boreholes to examine it for dye penetration. Upon coring through to the ocean, the pond level dropped 4 cm, confirming that the pond had been above sea level throughout the test. Dye experiments in the pond proved messy and cores removed from beneath the dyed pond water became briefly submerged in dye their entire length during extraction. Shaving off the core exterior using a sharp knife, however revealed the dye's actual vertical penetration (see photo in Figure 12). We found that dye had penetrated into, but not through the remaining ice in the 31, 45, and 61 cm bores, and had likely penetrated through the ice completely in the 81 cm bore. In each case, dyed pond water had refrozen in small channels within the interior of the ice. The dye penetration was greatest in the shallowest bore, where it was penetrating into the warmest ice, and least in the 61 cm bore where it was penetrating into the coldest ice. Dye penetrated through all the recovered portion of the core from the 81 cm bore, but approximately 15 cm of this core was lost during extraction. Unlike in the unaltered pond bottom test where dye permeated the porous upper ice but did not travel deep into the ice interior along select pathways, the dye was conducted deep into small

channels during this test. Green dye found saturating the bottom part of the ice recovered from the bottom of the 31, 45, and 61 cm bores appeared to have infiltrated during the extraction stage, as dye did not appear to penetrate the whole of the cold interior of the ice. It is also possible that some pathway conducted dye all the way through the ice for a brief time before the dyed water froze, blocking percolation. The behavior of the dyed water in the pond bottom appeared to indicate that the removal of the upper core section had provided access to connective pathways that had not previously reached all the way to the surface of the ice.

These results show two interesting aspects of the percolation behavior. First, the percolation blockage process makes the pond bottom self-healing. Bore holes, which mechanically opened access to new percolation pathways, were resealed quickly, before substantial pond water volume could drain through them. In the natural evolution of a pond, this is equivalent to the capability to block new pathways made connective by enlargement of brine space due to internal melt, or due to removal of impermeable surface layers, so long as the ice conditions remain cold enough. In other words, connective pore structures that form in the bottom of ponds are likely to be repaired during the early part of the melt season at a rate strongly guided by the present temperature of the ice. The mechanism of percolation blockage could therefore directly relate to ice temperature and pond water mass balance.

The second significant finding is that we did not locate a discrete impermeable layer within which all pores had been already blocked by prior water infiltration—even though the pond level was above sea level. Instead, it appears that percolation blockage already in place when we arrived at the pond had occurred at a variety of depths within the ice. Mechanically removing of the upper portion of the ice by coring opened newly accessible percolation pathways at all depths tested—presumably by providing access to pathways that had not yet connected to the surface as well as by removing the portion of pathways blocked by prior freshwater plugs.

4. Discussion

4.1. Importance for Pond Formation and Enduring Impacts

Our results illustrate several aspects of the percolation blockage process in first year sea ice. We illustrate our key findings regarding how the process works in Figure 13. Warming of ice in the spring makes many connective pathways in the brine structure of the ice (see changes between Figures 13a and 13b). When the infiltration of fresh meltwater into sea ice begins (Figure 13c), the water encounters lower temperatures in the ice interior and ice accretion occurs in percolation pathways. This seals the ice against further water percolation. While processes such as superimposed ice formation may also affect ice permeability, percolation blockage continues to restrict percolation through the sea ice after the removal of superimposed ice and appears necessary to explain observed first year ice pond evolutions [*Polashenski et al.*, 2012; *Landy et al.*, 2014]. Our investigation of this mechanism indicates that percolation blockage causes the ice to behave in a self-repairing manner, blocking new percolation pathways established so long as the ice remains sufficiently cold and the intruding water remains sufficiently fresh. The result is that percolation blockage permits ponds to form above sea level—solving the conundrum about ponds forming on highly permeable ice discussed in the introduction. Better still, the result provides a mechanistic connection between conditions forcing ice temperature and melt pond formation.

The duration that ponds can remain elevated above sea level (staying in the phase indicated by Figure 13c rather than moving to 13d) has important direct and indirect impacts for Arctic sea ice albedo, energy balance, and light availability in the upper ocean. Above-sea-level ponding substantially increases the area of ice covered by ponds, often by 10s of percentage points, appreciably lowering albedo [*Perovich et al.*, 2002; *Polashenski et al.*, 2012; *Perovich and Polashenski*, 2012; *Landy et al.*, 2014]. The enhancement of solar absorption caused by this albedo reduction has been estimated at tens of centimeters of ice melt equivalent per week [*Polashenski et al.*, 2012]. The duration of time that widespread above sea level ponding persists varies from several days to several weeks on first year ice, meaning the direct energy impact of above-sea-level pond formation is a significant factor in variability of annual ice mass balance [*Polashenski et al.*, 2012; *Landy et al.*, 2014].

The impacts of early, above-sea-level pond coverage also endure well beyond the time when ponds drain to sea level. Once the ponds drain to sea level, the extent of ponds that remain is dictated by the area of the ice surface lying below sea level [*Polashenski et al.*, 2012; *Landy et al.*, 2014]. Before melt onset, there are
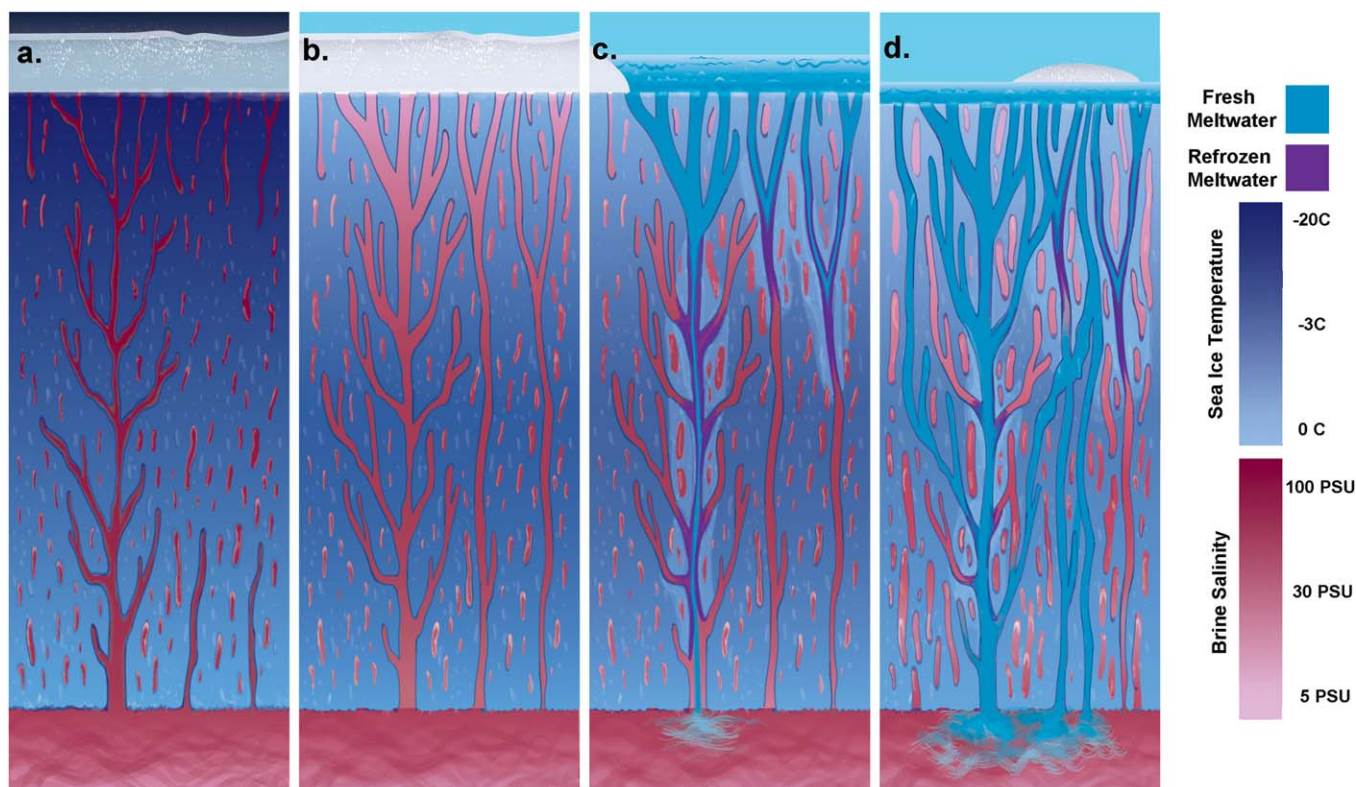
Figure 13. A schematic illustration of the percolation process at four times during the seasonal evolution. At the top a dark, (a) snow covered winter scene changes to a light and (b) snow covered spring scene. (c) Ponds then form above sea level and (d) eventually drain to sea level. Sea ice beneath is represented in shades of blue-grey, with darker tones representing colder ice (see approximate temperature scale at right). Brine and ocean water, are represented in shades of red, with darker tones representing higher salinity. Intruding fresh melt is represented as light blue and refrozen melt is represented as purple. The schematic is not to scale. To show detail, the horizontal dimension of brine inclusions are substantially stretched relative to the vertical dimension—hence brine inclusions larger than would be expected occupy a higher fraction than would be expected. (a) Winter sea ice prior to the onset of melt. Cold ice temperatures, particularly in the upper ice, result in low brine volumes at high concentration. Brine inclusions are mostly isolated from one another. Brine drainage channels organized by convective desalination are the exception, forming large arborescent structures at decimeter-scale intervals. See *Cole and Shapiro* [1998] for images of these larger inclusions. (b) Spring sea ice shortly before the onset of surface melt. Ice temperature has warmed to greater than −3℃, and brine inclusions have grown to the point where many are interconnected. The ice interior is coldest and least connected. Multiple potential percolation pathways of various sizes exist from the ice surface to the ocean. (c) Snow melt begins. Freshwater begins percolating into connective pathways, encountering ice that is below 0℃. Ice immediately begins accreting on the walls of brine channels. The new ice forms at a variety of depths and soon blocks percolation in all but exceptionally large channels. Latent heat from the refreezing snowmelt warms the area surrounding the newly forming ice. Adjacent brine pockets enlarge to maintain their salinity at the freezing point, sometimes creating alternative pathways for percolation, which are subsequently blocked as well. (d) Continued warming of the ice causes internal melt and raises brine volume. Surface melt removes some blockages. Many more pathways become connective, including many smaller pathways. As each pathway becomes connective, freshwater rushes in from above. The ice is warmer now and though ice begins accreting on the walls of the pathway, channels no longer block reliably. Percolation begins at many locations. The ice can no longer support above sea level ponds.

typically very few areas on undeformed first year ice whose surface is near to or below sea level. Though snow dunes create notable surface topography and observations show that ponds typically initially form in the locations of lower surface elevation between snow dunes [*Petrich et al.*, 2012], even these areas are generally above sea level prior to melt onset [*Polashenski et al.*, 2012]. Later in the melt season, pond locations are overwhelmingly confined to the depressions where early season melt feedbacks created ice surfaces below sea level [*Polashenski et al.*, 2012; *Landy et al.*, 2014]. Above-sea-level ponds, therefore, provide the crucial service of creating below-sea-level depressions that can remain ponds after drainage by lowering albedo and accelerating melt in the ponded areas. Without the formation of early season ponds to create these depressions, little or no area of the ice surface would be below sea level late in the season and pond coverage would be lower or absent.

4.2. A Link Between Forcings and Variability in Pond Formation on First Year Ice

Percolation blockage appears to provide an intrinsic link in the ice-albedo feedback, connecting variability in forcing conditions with variability in pond formation on first year ice. Our results show that percolation blockage is highly dependent on the salinity of percolating meltwater and the internal temperature of the ice. The implication is that the mass of snow available for melt (which is likely the most significant control

over the salinity of the meltwater) and trajectory of spring warming prior to melt onset (which sets the internal ice temperature when meltwater begins forming) likely have tremendous implications for the energy balance of the summer Arctic sea ice. Evaluating these connections holds the potential to greatly improve our understanding of floe to floe, interannual, and climatological variability in pond formation.

4.2.1. Spring "Abruptness"

The surface melt onset and internal ice warming are not necessarily synchronous. Melt onset tends to be driven by synoptic events [*Mortin et al.*, 2016] and can be initiated abruptly. Internal ice temperature is controlled by all aspects of local surface energy balance and the penetration of solar radiation integrated over a longer time frame. In terms of interannual variability, an anomalously early or abrupt melt onset will result in meltwater creation atop colder ice than an anomalously late or gradual melt onset. When melt occurs atop colder ice with smaller brine inclusions, the ability of freshwater to block against percolation is increased, enhancing the formation of ponds. Conversely, when ice warms substantially before meltwater is formed, percolating meltwater will encounter large flaws and little remaining heat capacity for refreezing, resulting in shorter duration of above-sea-level pond formation. In addition to variability, trends that could either increase or decrease ice temperature at melt onset seem likely in a warming climate. Earlier melt onset, for example, would shorten the time between polar sunrise and melt onset. This would reduce the duration of time that spring sunlight penetrates into and warms the ice interior prior to pond formation and result in melt initiation atop less porous ice. Higher winter temperatures, on the other hand, might result in higher spring ice temperatures. The net effect of all the factors impacting ice internal temperature, such as ocean heat flux and minimum winter temperatures, is uncertain.

The spring transition during the year of our observations appears to have had an unusually slow progression. Temperatures were near the freezing point for several weeks during our experiment but pond formation did not begin until we were leaving (see discussion of weather in section 2). Minimum ice temperatures at this time ($-1.3°C$ to $-0.9°C$) were warmer than those observed at melt onset during prior experiments tracking melt pond evolution of up to $-1.8°C$, [*Polashenski et al.*, 2012] and up to $-2.8°C$ [*Landy et al.*, 2014]. Further comparison, provided by ice temperature data from the thermistor string data collected by the Barrow Ice Observatory [*Druckenmiller et al.*, 2009], is presented in Figure 14. Minimum interior ice temperature at the onset date of melt pond formation at the Barrow site has varied from $-2.9°C$ to $-1.6°C$ from 2008 to 2014 with no clear trend. Detailed pond coverage observations throughout the melt are only available from 2008–2010 and 2012 at Barrow [*Polashenski et al.*, 2012], and from 2011 and 2012 in the Canadian Archipelago [*Landy et al.*, 2014]. In this limited data set, however, the duration that above-sea level ponds endured corresponds well to the minimum ice temperature at the onset of ponding (Figure 13c), supporting the hypothesis that interannual variability in ice temperature at the onset of melting may play a major role in pond development. We hypothesize, based on the slow spring transition and warm ice temperatures prior to pond formation, that analysis of pond coverage being conducted by others will show lower than typical pond coverage in 2014 in the late melt onset areas of the Chukchi region.

4.2.2. Snowpack Water Content

The availability of fresh meltwater for percolation blockage on first year ice is dependent on the mass of snowmelt, as well as rainfall and melt of already-desalinated ice. Rainfall during the brief pond formation period is not expected to be a major contributor relative to snowmelt mass in most years. Sea ice melt is varies in salinity as desalination occurs but would be expected to exhibit only limited interannual variability compared to snow water equivalent. On this basis, we reason snowpack mass is likely the source with the most control over floe to floe and year to year variability in salinity of percolating meltwater on first year ice.

Arctic sea ice snowpack depths on individual floes have been observed to range from near zero to over 50 cm, with density near 340 kg/m^3, producing water content varying from near zero to over 15 cm [e.g., *Warren et al.*, 1999; *Webster et al.*, 2014; *Sturm et al.*, 2002]. The snowpack is subject to both interannual and climate variability and can exhibit large floe-to-floe variability due to wind redistribution or variation in ice formation date (e.g., late formation that causes a floe to miss autumn snows). Without a sufficient snow pack, we hypothesize first year ice may lack the freshwater required for sealing and therefore not form ponds or permit earlier pond drainage. A lack of snow would also result in greater penetration of solar radiation into the ice, resulting in greater internal heat absorption and more rapid brine space enlargement. Prior work has also connected thinner snowpacks to lower formation of superimposed ice [*Eicken et al.*, 2004], reducing the presence and persistence of this preliminary barrier to percolation. This work (section 3.6)
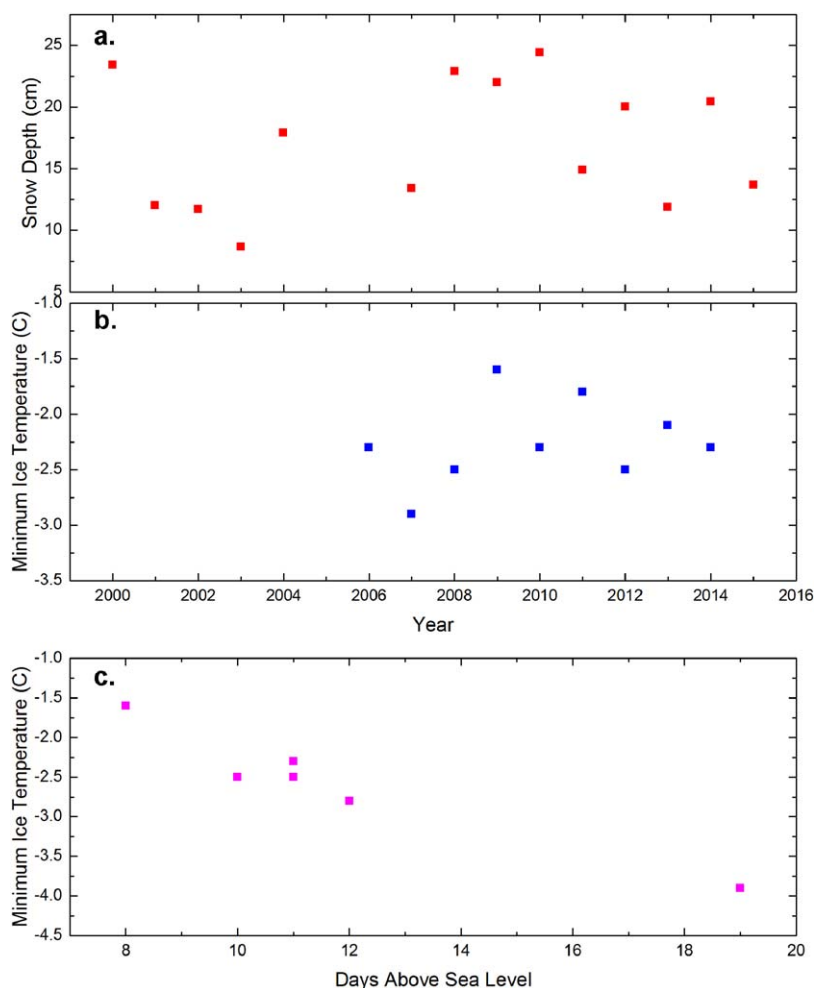
Figure 14. (a) Mean snow depth at the end of winter and (b) minimum ice temperature at the onset of ponding from several years of observations at Barrow, AK give an idea of the variability in these parameters. (c) Minimum internal temperature of the ice at the onset of pond formation, plotted against duration of above-sea level ponding, based on data presented in *Polashenski et al.* [2012] for Barrow, AK and *Landy et al.* [2014] for Resolute Bay, Canada. Though the number of observations available is limited, we find that correlation between minimum internal ice temperature at the onset of ponding and duration of above sea level ponding is strong and statistically significant. ($R^2 = 0.91$, $p = 0.002$).

demonstrates that water of lower salinity is able to block percolation later in the melt season. Most signs, therefore, suggest thinner snowpacks will result in shorter duration of above-sea level ponding. In the extreme, pond formation may not occur at all. Anecdotal observation supports this possibility, indicating that on a sea ice runway, where snow was artificially cleared throughout winter, pond formation was very limited, despite extensive ponding nearby [*Eicken et al.*, 2004]. Observations of large, flat, first year sea ice floes occasionally remaining largely unponded late in the melt season suggest this can happen naturally at times (see Figure 15 herein, and also in *Perovich et al.* [2002], Figure 12). In these cases, a pathway of melt may exist where the ice is not able to block percolation at melt onset due to a lack of fresh water, early sea-son ponds never form to create below-sea-level depressions, and pond coverage remains very low. The pre-melt conditions of the particular floes that have been observed with very limited pond formation are generally unknown, but the unponded floe in Figure 15 appears to be thinner ice with no evidence of snow cover (i.e., no snow dunes unlike the ponded floe at right). We examined one floe that may have been of this type before the melt season (Station 75, 28 May). The floe had a mean snow depth of only 6.5 cm, a high minimum internal ice temperature relative to other floes we had examined at that time ($-1.6°C$), and a very high porosity. Ice thickness was somewhat thinner but still within the variability of the other sites, at 0.76 m. Removing full cores, we found centimeter-scale porosity penetrating through even the interior of the ice (see Figure 16). The large porosity was likely due to internal solar heating, but also may have been
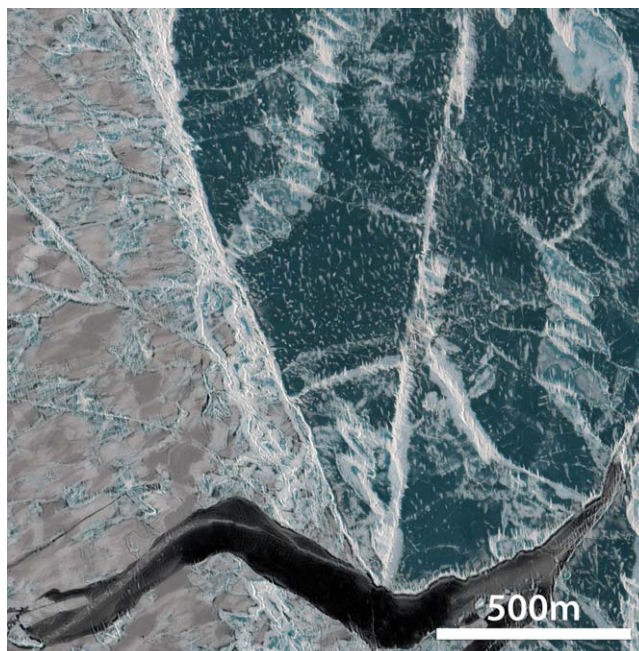
Figure 15. Satellite image of a multikilometer area of ice which has not experienced ponding, while surrounding ice is at the peak of spring pond coverage. Image is from 13 June 2014 at 72.00°N 128.00°W in the Beaufort Sea. ©2015 DigitalGlobe NextView License.

due to a high salinity associated with rapid growth. We tried extensively to demonstrate percolation blockage in slug tests using fresh water with no success. Formation of ponds above sea level on this floe seemed highly improbable.

In addition to floe to floe variability, the influence of interannual variability and climatological trends in the sea ice snowpack should be considered. We plot snow depth observations from the Barrow Ice Observatory site in Figure 14 from 2000 to 2014 to demonstrate the level of this interannual variability at one site [*Druckenmiller et al.*, 2009]. Each year's snow depth is the represented as the mean of 200–2000+ observations collected along transects 200–2000 m in length. Transects were conducted in a variety of configurations but were designed to capture the mean and variability of snow depth at the end of winter on level landfast ice. In general, data sets

containing more than 200 points are oversampled, such that all data sets capture mean and variability well. Mean end-of-winter snow depth varies substantially, from 7 to 24 cm, during this period. Spatial variability in snow depth from region to region is likely of similar or greater magnitude [*Warren et al.*, 1999; *Webster et al.*, 2014]. Indications of long-term trends in sea ice snowpack are as yet very uncertain, though available data suggests snow pack depth is decreasing [*Webster et al.*, 2014]. Unfortunately, the available observations do not permit us to comment confidently on the sensitivity of pond formation to snowpack depth or water content. Future studies will need to examine whether the need for fresh water to block percolation can be satisfied fully by only a small amount of freshwater (i.e., binary behavior) or whether the snowpack might have incremental impacts over a broad range of snow depths realized by additional freshwater extending the duration of above-sea-level ponding.

4.3. Current Model Representation of Percolation Processes

The manner in which melt ponds are currently represented in models is an important consideration in evaluating the importance of these results. Most physically based model representations of melt ponds currently include a scheme in which meltwater retention volume is tracked and the retained volume is distributed into ponds based on a parameterized treatment of ice surface topography [e.g., *Hunke et al.*, 2013, 2015; *Flocco et al.*, 2010, 2012; *Skyllingstad et al.*, 2009]. Parameterizations of surface topography, though improving [*Hunke et al.*, 2013], tend to be rudimentary and limited by a lack

Figure 16. Image of a core section showing centimeter+ scale pore space common in deteriorating ice.

of observations of sea ice surface roughness, while melt water balance is based on a physical scheme. Most of the schemes for calculating meltwater retention seek to exploit relationships proposed in *Golden et al.* [2007] between Darcy permeabilities of sea ice and ice characteristics as a means for calculating water retention [e.g., *Hunke et al.*, 2015]. The evidence we present, however, shows that these relationships do not always hold for first year ice. The existing relationships were determined from theoretical modeling and limited empirical tests that used *seawater* as the test fluid, and do not capture the behavior of sea ice permeability in the presence of fresh water intrusion very well. As we demonstrated in section 3, intruding freshwater can rapidly modify the Darcy permeability of first year sea ice with minimal impact on bulk porosity. The ice is, therefore, not a medium with a fixed permeability-porosity relationship and this aspect of current permeability representations is not physically supported. The upshot is that the existing schemes may be easily adapted to these new findings by incorporating percolation blockage as a reduction in permeability constant based on other variables for first year ice. Both ice temperature and snowpack water content are explicitly tracked in nearly all global climate models, providing a ready path for physics-based parameterizations of percolation blockage. We expect further research will enable development of a parameterization relating percolation blockage to both of these variables. In section 4.4, we evaluate the available evidence and suggest a possible relationship to ice temperature.

It is important to note that despite this inclusion of a nonphysical permeability porosity relationship, the latest versions of several GCM's produce melt pond coverage evolution broadly comparable to the limited available observations [e.g., *Hunke et al.*, 2013]. This is somewhat surprising. Based on the Darcy's law applications used, we expect the *Golden et al.* [2007] porosity-permeability relationship to produce pond drainage rates rapid enough to prohibit pond growth on first year ice. Using porosity values, we observed in first year sea ice at the onset of pond formation ($\phi > 0.1$), and a (lower than expected) hydraulic head for the ice surface of $\Delta h = 0.05$ m, for example, would result in the loss of ~ 0.07 m/d of meltwater through 1 m thick. We arrive at this according to

$$\Delta V = 3\phi^3 \ x \ 10^{-8} * \frac{Ag\rho\Delta h}{\mu L} * \Delta t, \tag{10}$$

where the relationship for the permeability constant $k = 3\phi^3 \times 10^{-8}$ is from *Golden et al.* [2007], *A* is the flow area, *g* is the gravitational constant, ρ is the density of water, μ is the kinematic viscosity of water, *L* is the thickness of the ice, and Δt is the time elapsed. The success of the models, therefore, is likely due to counteracting factors. Possible factors vary by model and a thorough investigation is beyond the scope of this study. Factors that may be important however, include the modeled bulk salinity and temperature of the ice, ice topography, and pond water drainage formulation. In particular, the manner in which topography is handled may permit pond water to be retained without hydraulic head in some schemes, particularly those that use rigid treatment of ice [e.g., *Flocco et al.*, 2010]. At least one model also appears to have partly replaced the permeability-porosity drainage model with an empirical drainage formula based on pond depth [*Hunke et al.*, 2013]. Since the use of the empirical formulation is triggered anytime the drainage determined by Darcy's law exceeds the empirical formulation this serves as a constraint on excess drainage.

Exploring the impact that revised physics could have on melt pond coverage predicted by GCM scale models is beyond our scope here, but there is evidence that capturing early season permeability blockage correctly is important to predicting the evolution of pond coverage. Process-scale modeling of melt pond behavior indicates that representing the processes that restrict permeability to near zero during early melt enables more accurate capture of early season surface flooding behavior. *Skyllingstad et al.* [2015] tested the addition of a meltwater refreezing process in a resolved-scale sea ice melt pond model. In these tests, the model generates impermeable layers when fresh melt percolates into the ice using salinity-temperature dynamics. The permeability blockage produced is of similar duration to that expected from our observations, though the manifestation is nearer the surface, more discrete than we observe, and includes ice formation we would recognize as superimposed ice later into melt than seen in studies we cite here. Mushy layer physics in some current melt pond GCM's may produce similar layers, and we speculate that these too may partly compensate for incorrect percolation physics. Further improvements of the process model since *Skyllingstad et al.* [2015] have enabled us to instead produce internal freezing when fresh water begins to intrude from the surface. In either case, by capturing the behavior that ice becomes impermeable for a duration of time after melt onset, and ensuring the model physics produced the correct duration of

impermeable behavior, the model was able to reproduce key features of the pond coverage evolution including the early season flooding peak and subsequent pond drainage. Model sensitivity studies showed that snow depth also had a significant effect on the resulting pond fraction both during the flood stage and after drainage, in part through controls on the formation of these impermeable layers. The timing of pond drainage to sea level was found to be sensitive to the choice of permeability coefficient in the permeable ice and solar absorption in the layers where refreezing had occurred. A permeability coefficient of 1×10^{-10} was required to accurately simulate pond behavior. This suggests the percolation through meltwater-modified brine channels may not obey existing Darcian flow models. The success in modeling the overall character of the spring melt pond evolution, however, is very encouraging, and the model sensitivity runs clearly demonstrated that small errors in the duration of impermeable behavior had large and lasting impacts on seasonal albedo.

4.4. Potential First-Order Representation of Percolation Blockage in Models

Our discussion of variability in ice temperature at melt onset and snow water content on sea ice in section 4.2 reflects the paucity of data available on both. Because of this lack of data, it is not yet possible to make conclusions about how trends in these forcing conditions may be creating a trend in pond coverage. Nevertheless, the relationship between these variables and pond formation outlines a powerful mechanism for pond control that we feel should, eventually, be represented in melt pond models as physical realism continues to be improved. After considering the available data, we concluded there is enough evidence available to propose a possible empirical means to quantitatively relate pond formation and ice temperature in models. We propose this mechanism to encourage the collection of additional observations that can test it and encourage efforts to represent permeability transitions in sea ice models and evaluate their importance.

The suggestion is to simply incorporate percolation blockage according to thresholds of minimum ice temperature. We propose to divide meltwater retention into stages of: (1) zero drainage, (2) drainage based upon a finite permeability (provided by existing Darcian schemes), (3) and unrestricted drainage fixing ponds to sea level. The transitions would be dictated by internal ice temperature. We find agreement across the three available sources [*Polashenski et al.*, 2012; *Landy et al.*, 2014; and this work] for a minimum ice temperature threshold of approximately $-1.6°C$ for the first transition, when some water losses begin, and $-0.9°C$ for the second, at which percolation blockage is no longer possible. The first transition temperature is the ice temperature at which prior observations in the Chukchi and Canadian Archipelago [*Polashenski et al.*, 2012; *Landy et al.*, 2014] both saw the initiation of meltwater loss at macroscopic holes. These macroscopic holes likely enlarged from exceptional brine channels not blocked by percolating fresh water. The coldest single hole at which our fresh water tests were unable to produce percolation blockage also exhibited this minimum temperature. The second transition, occurring when minimum ice temperature reaches $-0.9°C$, reflects the ice temperature when the onset of large-scale ice permeability was noted in meltwater balance studies by *Polashenski et al.*, 2012 and *Landy et al.*, 2014. Our in situ tests agreed closely, demonstrating difficulty in achieving percolation blockage at some holes when ice temperature exceeded $-1.3°C$, and at all holes at above $-0.9°C$.

These temperature thresholds simplify the process we have described greatly, not taking into account the role of solar penetration or snow pack in any way. Nevertheless, they permit above-sea-level pond formation, and enable this behavior to be connected to ice temperature; improving realism over current schemes, which may incorporate nonphysical permeability-porosity relationships. More detailed investigations of the relationship between snow pack and the process of percolation blockage are needed to develop more complex relationships accounting for fresh water volume.

5. Conclusions

We have directly demonstrated the existence of the process of percolation blockage in sea ice and shown that this process is critical to the formation of melt ponds atop otherwise highly permeable sea ice. The process blocks percolation of fresh meltwater through the otherwise connective pore structure of first year Arctic sea ice. The blockage reduces fluid permeability to near zero and permits melt ponds to form and remain above sea level. Demonstration of the process affirms prior observations [*Polashenski et al.*, 2012] that indicated an internal freezing process was necessary to explain the observed hydraulic balance of

ponds and the evolution of temperature and salinity in the ice observed during some field experiments [*Landy et al.*, 2014]. The results, therefore, reconcile observations of high permeability in sea ice with the observation that ponds form above sea level by identifying why the permeability deviated from expectations. Theoretical relationships between porosity and permeability depend on a random distribution of the pore space. We observe that ice accretion occurs preferentially in connective pathways during meltwater intrusion, changing the ice pore structure in a nonrandom manner and causing deviation from established porosity-permeability relationships.

After identifying the mechanism, additional tests showed that the impact of internal ice accretion on ice permeability is principally dependent on ice temperature and intruding water salinity. The ice temperature at melt onset is dependent on the "abruptness" of the transition from cold winter conditions to spring melt and the salinity of intruding water is dependent, at least in part, on the amount of snow available for fresh melt production. Changes in these variables can have a profound impact on the summer evolution of melt ponds and therefore over seasonal ice mass balance. In the extreme, anecdotal evidence suggests a divergent path for first year sea ice with very low snowpack that does not lead to melt pond formation at all, due to a lack of fresh water for percolation blockage. Within more common bounds, we show that observed levels of regional and interannual variability of ice temperature at melt onset and end of winter snow have the potential to exert significant impacts on pond formation and sea ice summer energy balance. In particular, the limited quantitative evidence available from observations of ponds on first year ice supports the hypothesis that ponds remain above sea level longer, and therefore cover a greater time-averaged spatial extent in years of early melt onset occurring atop colder ice. This potentially adds another mechanism to the powerful albedo feedbacks associated with early melt onset. Climatological trends in both snow water content and ice temperature at melt onset are also likely, and could therefore drive trends in melt pond formation. Observations are currently insufficient to comment on the direction of these trends, highlighting another reason for interest in ice temperature monitoring and snow-on-sea ice climatology.

The connection between forcing conditions and summer ice albedo created by percolation blockage represents a physical mechanism that may provide a significant opportunity for model improvement. We find that additional evaluation of the relationships between snow water equivalent, ice temperature, and percolation blockage are will be required to produce a model parameterization that can correctly handle the deviation from the *Golden et al.* [2007] porosity-permeability relationship that intruding meltwater creates. In the interim, however, process model results suggest that relatively crude inclusion of a percolation blockage process can appreciably improve model representation of melt ponds by reproducing an impermeable behavior necessary to produce above sea level ponds. We find very close agreement between our experimental observations of percolation blockage and two prior observations of ice temperatures and pond behavior in different regions. This suggests transitions in percolation blockage behavior occur near specific temperatures. From these observations we suggest minimum ice temperature thresholds of $-1.6°C$ and $-0.9°C$ as appropriate levels to transition ice permeability from zero to a finite value and from a finite value to unrestricted flow in a first-order empirical model capturing the impact of percolation blockage. These observed thresholds may be used with caution in parameterization of meltwater balance or used as checkpoints to compare more sophisticated mushy layer physics models against.

We suggest future work should be undertaken in field and laboratory settings to better describe the nature of connective pathways in sea ice and the blockage processes occurring within them. Development of a more detailed relationship describing the thermohaline dynamics of meltwater percolation will likely yield significant dividends in improving predictability of sea ice on a seasonal scale.

References

Arrigo, K. R., et al. (2012). Massive phytoplankton blooms under Arctic sea ice, *Science*, *336*(6087), 1408–1408.

Cole, D. M., and L. H. Shapiro (1998), Observations of brine drainage networks and microstructure of first-year sea ice, *J. Geophys. Res.*, *103*(C10), 21,739–21,750.

Cole, D. M., H. Eicken, K. Frey, and L. H. Shapiro (2004), Observations of banding in first-year Arctic sea ice, *J. Geophys. Res.*, *109*, C08012, doi:10.1029/2003JC001993.

Curry, J. A., J. L. Schramm, and E. E. Ebert (1995), Sea ice-albedo climate feedback mechanism, *J. Clim.*, *8*(2), 240–247.

Druckenmiller, M. L., H. Eicken, M. Johnson, D. Pringle, and C. Williams (2009),Towards an integrated coastal sea-ice observatory: System components and a case study at Barrow, Alaska, *Cold Re. Sci. Technol.*, *56*(1–2), 61–72.

Eicken, H., W. B. Tucker, and D. K. Perovich (2001), Indirect measurements of the mass balance of summer Arctic sea ice with an electromagnetic induction technique, *Ann. Glaciol.*, *33*(1), 194–200.

Eicken, H., H. R. Krouse, D. Kadko, and D. K. Perovich (2002), Tracer studies of pathways and rates of meltwater transport through Arctic summer sea ice, *J. Geophys. Res.*, *107*(C10), 8046, doi:10.1029/2000JC000583.

Eicken, H., T. C. Grenfell, D. K. Perovich, J. A. Richter-Menge, and K. Frey (2004), Hydraulic controls of summer Arctic pack ice albedo, *J. Geophys. Res.*, *109*, C08007, doi:10.1029/2003JC001989.

Flocco, D., D. L. Feltham, and A.K. Turner (2010), Incorporation of a physically based melt pond scheme into the sea ice component of a climate model, *J. Geophys. Res.*, *115*, C08012, doi:10.1029/2009JC005568.

Flocco, D., D. Schroeder, D. L. Feltham, and E. C. Hunke (2012), Impact of melt ponds on Arctic sea ice simulations from 1990 to 2007, *J. Geophys. Res. Oceans*, *117*(C9).

Frankenstein, G., and R. Garner (1967), Equations for determining the brine volume of sea ice from-0.5 C to-22.9 C, *J. Glaciol.*, *6*, 943–944.

Freitag, J., and H. Eicken (2003), Meltwater circulation and permeability of Arctic summer sea ice derived from hydrological field experiments, *J. Glaciol.*, *49*(166), 349–358.

Frey, K. E., D. K. Perovich, and B. Light (2011), The spatial distribution of solar radiation under a melting Arctic sea ice cover, *Geophys. Res. Lett.*, *38*, L22501, doi:10.1029/2011GL049421.

Golden, K. M. (2003), Critical behavior of transport in sea ice, *Physica B*, *338*(1), 274–283.

Golden, K. M., S. F. Ackley, and V. I. Lytle (1998), The percolation phase transition in sea ice, *Science*, *282*(5397), 2238–2241.

Golden, K. M., H. Eicken, A. L. Heaton, J. Miner, D. J. Pringle, and J. Zhu (2007), Thermal evolution of permeability and microstructure in sea ice, *Geophys. Res. Lett. 34*, L16501, doi:10.1029/2007GL030447.

Hunke, E. C., D. A. Hebert, and O. Lecomte, (2013), Level-ice melt ponds in the Los Alamos sea ice model, CICE, *Ocean Modelling*, *71*, 26–42.

Hunke, E. C., W. H. Lipscomb, A. K. Turner, N. Jeffery, and S. Elliott (2015), *CICE: The Los Alamos Sea Ice Model Documentation and Software User's Manual Version 5.1 LA-CC-06-012*, Los Alamos Natl. Lab., Los Alamos, N. M.

Landy, J., J. Ehn, M. Shields, and D. Barber (2014), Surface and melt pond evolution on landfast first-year sea ice in the Canadian Arctic Archipelago, *J. Geophys. Res. Oceans*, *119*, 3054–3075, doi:10.1002/2013JC009617.

Marshall, H. P., G. Koh, M. Sturm, J. B. Johnson, M. Demuth, C. Landry, J. Deems, and J. A. Gleason (2006), Spatial variability of the snowpack: Experiences with measurements at a wide range of length scales with several different high precision instruments, in *Proceedings ISSW*, International Snow Science Workshops, pp. 359–364.

Mortin, J., G. Svensson, R. G. Graversen, M.-L. Kapsch, J. C. Stroeve, and L. N. Boisvert (2016), Melt onset over Arctic sea ice controlled by atmospheric moisture transport, *Geophys. Res. Lett.*, *43*, 6636–6642, doi:10.1002/2016GL069330.

Nicolaus, M., C. Katlein, J. Maslanik, and S. Hendricks (2012), Changes in Arctic sea ice result in increasing light transmittance and absorption, *Geophys. Res. Lett.*, *39*, L24501, doi:10.1029/2012GL053738.

Perovich, D. K., and C. Polashenski (2012), Albedo evolution of seasonal Arctic sea ice, *Geophys. Res. Lett.*, *39*, L08501, doi:10.1029/2012GL051432.

Perovich, D. K., T. C. Grenfell, B. Light, and P. V. Hobbs (2002), Seasonal evolution of the albedo of multiyear Arctic sea ice, *J. Geophys. Res.*, *107*(C10), 8044, doi:10.1029/2000JC000438.

Petrich, C., P. J. Langhorne, and Z. F. Sun (2006), Modelling the interrelationships between permeability, effective porosity and total porosity in sea ice, *Cold Reg. Sci. Technol.*, *44*(2), 131–144.

Petrich, C., H. Eicken, C. M. Polashenski, M. Sturm, J. P. Harbeck, D. K. Perovich, and D. C. Finnegan, (2012), Snow dunes: A controlling factor of melt pond distribution on Arctic sea ice, *J. Geophys. Res.: Oceans*, *117*(C9).

Polashenski, C., D. Perovich, and Z. Courville (2012), The mechanisms of sea ice melt pond formation and evolution, *J. Geophys. Res.*, *117*, C01001, doi:10.1029/2011JC007231.

Skyllingstad, E. D., C. A. Paulson, and D. K. Perovich (2009), Simulation of melt pond evolution on level ice, *J. Geophys. Res.*, *114*, C12019, doi:10.1029/2009JC005363.

Skyllingstad, E. D., K. M. Shell, L. Collins, and C. Polashenski (2015), Simulation of the melt season using a resolved sea ice model with snow cover and melt ponds, *J. Geophys. Res. Oceans*, *120*, 5194–5215, doi:10.1002/2014JC105569.

Stroeve, J. C., T. Markus, L. Boisvert, J. Miller, and A. Barrett (2014), Changes in Arctic melt season and implications for sea ice loss, *Geophys. Res. Lett.*, *41*, 1216–1225, doi:10.1002/2013GL058951.

Sturm, M., and J. A. Holmgren (1999), Self-recording snow depth probe, U.S. Patent No. 5,864,059, U.S. Patent and Trademark Off., Washington, D. C.

Sturm, M., J. Holmgren, and D. K. Perovich, (2002), Winter snow cover on the sea ice of the Arctic Ocean at the Surface Heat Budget of the Arctic Ocean (SHEBA): Temporal evolution and spatial variability, *J. Geophys. Res.: Oceans*, *107*(C10).

Warren, S. G., I. G. Rigor, N. Untersteiner, V. F. Radionov, N. N. Bryazgin, Y. I. Aleksandrov, and R. Colony (1999), Snow depth on Arctic sea ice, *J. Clim.*, *12*(6), 1814–1829.

Webster, M. A., I. G. Rigor, S. V. Nghiem, N. T. Kurtz, S. L. Farrell, D. K. Perovich, and M. Sturm (2014), Interdecadal changes in snow depth on Arctic sea ice, *J. Geophys. Res. Oceans*, *119*, 5395–5406, doi:10.1002/2014JC009985.

Weeks, W. F., and S. F. Ackley (1986), The growth, structure, and properties of sea ice, in *The Growth, Structure and Properties of Sea Ice*. NATO ASI Series, edited by N. Untersteiner, pp. 9–164, Springer, New York, doi:10.1007/978-1-4899-5352-0.